NASA Technical Memorandum 101029

Control of a Human-Powered Helicopter in Hover

Joseph J. Totah and William Patterson

(NASA-TM-101029) CONTROL OF A HUMAN-POWERED HELICOPTER IN HOVER (NASA) 65 p CSCL 01C

N89-13438

Unclas

G3/08 0183253

November 1988

National Aeronautics and
Space Administration

NASA Technical Memorandum 101029

Control of a Human-Powered Helicopter in Hover

Joseph J. Totah, Ames Research Center, Moffett Field, California
William Patterson, California Polytechnic State University, San Luis Obispo, California

November 1988

NASA

National Aeronautics and
Space Administration

Ames Research Center
Moffett Field, California 94035

SYMBOLS

a	main rotor and control surface lift-curve slope, 1/rad
A	main rotor disk area, ft^2
C	main rotor and control surface chord, ft
c_{do}	section drag coefficient
C_L	lift coefficient
C_T	coefficient of thrust in ground effect
C_{T_∞}	coefficient of thrust out of ground effect
d	c.g. location from base of pilot compartment, ft
d_a	vertical distance from base of helicopter to hub, ft
d_b	vertical distance from base of helicopter to pilot c.g., ft
d_c	vertical distance from hub to rotor tip, ft
d_p	diameter of propellers, ft
D	total drag, lb
D_o	profile drag of the main rotors, lb
D_{cs}	profile drag of the control surfaces, lb
D_θ	differential perturbation gain, $1/sec^2$
D_ϕ	differential perturbation gain, $1/sec^2$
e	hinge offset (% main rotor radius)
F_r	control surface lift force of the rotor corresponding to $\psi_{t=0} = 0°$, lb
F_l	control surface lift force of the rotor corresponding to $\psi_{t=0} = 180°$, lb
g	gravitational acceleration, ft/sec^2
h	height from ground to average v_i location, ft
h_r	rotor tip height of the rotor corresponding to $\psi_{t=0} = 0°$, lb

h_l	rotor tip height of the rotor corresponding to $\psi_{t=0} = 180°$, lb
h_o	initial height of the base of the helicopter, ft
h_R	distance between c.g. and hub, ft
I_b	mass moment-of-inertia of one main rotor, slugs-ft^2
I_x	roll axis mass moment-of-inertia, slugs-ft^2
I_y	pitch axis mass moment-of-inertia, slugs-ft^2
K_a	differential height-to-angle gain of the control surface corresponding to h_r, rad/ft
K_b	differential height-to-angle gain of the control surface corresponding to h_l, rad/ft
$K_{c,1}$	roll feedback gain to roll acceleration, 1/sec^2
$K_{c,2}$	pitch feedback gain to roll acceleration, 1/sec^2
$K_{d,1}$	roll feedback gain to pitch acceleration, 1/sec^2
$K_{d,2}$	pitch feedback gain to pitch acceleration, 1/sec^2
l_{cs}	length of control surface, ft
L_v	lateral velocity stability, rad/sec/ft
L_p	roll damping, 1/rad/sec
m	total mass of the helicopter, slugs
m_b	mass of the pilot and pilot compartment, slugs
m_r	mass of one main rotor, slugs
m_t	mass at one rotor tip, slugs
M_q	pitch damping, 1/rad/sec
M_u	longitudinal velocity stability, rad/sec/ft
N	number of blades
N_r	yaw damping, 1/rad/sec
N_v	directional velocity stability, rad/sec/ft
p	body axis roll rate, rad/sec

$\dot{p}_{fb}$	roll acceleration feedback, rad/sec^2
q	body axis pitch rate, rad/sec
$\dot{q}_{fb}$	pitch acceleration feedback, rad/sec^2
r	body axis yaw rate, rad/sec
R	radius of main rotors, ft
R_e	effective radius of main rotors, ft
S_{cs}	contol surface area of one control surface, ft^2
t_{mr}	thickness of main rotors at 30% chord, ft
T	thrust required in ground effect, lb
T_∞	thrust required out of ground effect, lb
t	time, sec
u	body axis longitudinal velocity, ft/sec
u'	body axis longitudinal wind gust, ft/sec
v	body axis lateral velocity, ft/sec
v_i	induced velocity in ground effect, ft/sec
$v_{i\infty}$	induced velocity out of ground effect, ft/sec
w	body axis vertical velocity, ft/sec
w'	body axis vertical wind gust, ft/sec
W	weight, lb
X_q	change in X-force with respect to q, ft/sec/rad
X_u	longitudinal damping, 1/sec
Y_p	change in Y-force with respect to p, ft/sec/rad
Y_v	lateral damping, 1/sec
Z_w	vertical damping, 1/sec
β	beta, coning angle, rad

$\delta_{r,cs}$	rate and position limited control surface deflection of the rotor corresponding to $\psi_{t=0} = 0°$, rad
$\delta_{l,cs}$	rate and position limited control surface deflection of the rotor corresponding to $\psi_{t=0} = 180°$, rad
$\delta'_{r,cs}$	control surface deflection signal to actuators of the rotor corresponding to $\psi_{t=0} = 0°$, rad
$\delta'_{l,cs}$	control surface deflection signal to actuators of the rotor corresponding to $\psi_{t=0} = 180°$, rad
$\delta_{cs,d}$	differential control surface deflection, rad
γ	gamma, Lock Number
Ω	omega, rotor speed, rad/sec
ϕ	phi, body axis roll angle, rad
ψ	psi, body axis yaw angle, rad
ρ	rho, air density at sea level, slugs/ft^3
σ	sigma, solidity
θ	theta, body axis pitch angle, rad
θ_0	theta zero, main rotor initial pitch angle, rad
λ	inflow

SUMMARY

This report documents the study of a control system for the Da Vinci II human-powered helicopter in hovering flight. This helicopter has two very large, slowly rotating rotor blades and is considered to be unstable in hover. The control system is designed to introduce stability in hover by maintaining level rotors through the use of rotor tip mounted control surfaces. A five degree of freedom kinematic model was developed to study this control system and is documented in this report. Results of this study show the unaugmented configuration to be unstable due to the large Lock Number, and the augmented configuration to be stable.

The reason for NASA's involvement in this study (and the publication of this document) was so that instructors and students at the university level would have an educational aid for modeling and coding dynamic systems. The role of NASA in this study included the development and analysis of the kinematic model and control laws. Both analytical and numerical techniques were used.

INTRODUCTION

Since 1981 the California Polytechnic State University (Cal Poly, San Luis Obispo) student chapter of the American Helicopter Society has been involved in an effort to win the Igor Sikorsky Human-Powered Helicopter Design Competition prize. The requirements are to achieve human-powered hovering flight for 1 min, to reach an altitude of 3 m, and to stay within an area of 10 by 10 m. The first prototype, the Da Vinci I, was built of advanced composite materials and had two 50-ft-radius rotor blades which tapered from an 8-ft chord at the root to a 6-ft chord at the tip. The main rotors were driven by tip-mounted propellers that were 6-ft in diameter and turned at 350 rpm. The pilot supplied power to the propellers by winding-up string that was threaded through the main spars and wrapped around the shaft of the propellers. Rotor speeds up to 6 rpm could be obtained by this prototype.

The Da Vinci II differs from the Da Vinci I in that it features two 67-ft rotor blades having constant chords of 3 ft, refined advanced composite technology, tension cable reinforcement to reduce bending, and a unique control system concept.

Although the Da Vinci II was designed to sustain hover for 1 min, initial flight tests of the unaugmented configuration showed unstable dynamic behavior. One rotor tended to generate more lift than the other. The rotor generating less lift would eventually impact the ground in roughly 30 sec. The augmented configuration described in this report has not yet been flight-tested.

AIRCRAFT DESCRIPTION

The Da Vinci II is depicted in figure 1. The main spars are made from carbon-graphite, filament-wound composites. The rotor ribs are a sandwich type construction consisting of a styrofoam core covered with S-glass or graphite. The rotors are covered with Tedlar and the propellers mounted at the rotor tips were made by covering expandable foam with Kevlar cloth. The airfoil design of the main rotors is a Lissaman 7769 and the rotors are at a fixed incidence of 10°.

The control system consists of control surfaces mounted outboard of the tip mounted propellers. Optical sensors are mounted near each control surface in order to measure height from the ground. These control surfaces are differentially driven in proportion to the difference in height measured by the optical sensors. The control surfaces have the same airfoil shape as the main rotors and are actuated by servos mounted inside the spars.

The Da Vinci II has no tail rotor or any other conventional control mechanisms. The pilot compartment is rigidly attached to the shaft and hub, as are the main rotors.

MATH MODELS

A block diagram representation of the kinematic model and control system of the Da Vinci II is shown in figure 2. A description of the axis systems is given in Appendix A. The equations and principle assumptions used to describe both the kinematic model and the control system are presented in the next two sections. Special considerations and developments pertaining to the kinematic model are given in Appendix B.

Kinematic Model

This section contains modified, linearized perturbation equations of motion of a helicopter used as the kinematic model for the Da Vinci II. These equations were derived from the general equations of motion based on the following assumptions (ref. 1):

1. The flight condition is hover.

2. The rotors have a rectangular planform with no twist.

3. There are no stall or compressibility effects.

4. There is no higher harmonic rotor blade flapping.

5. There is no pitch-flap coupling.

6. The quasi-steady assumption is employed.

7. The vertical, longitudinal, and lateral axes are decoupled.

8. Small angle approximations are used.

A detailed discussion concerning the effects of aeroelasticity, rotor tip losses, and hovering in ground effect on the equations of motion for the Da Vinci II is given in Appendix B. The modified, linearized perturbation equations of motion based on the assumptions and special considerations are as follows:

$$
\begin{bmatrix} \dot{u} \\ \dot{\theta} \\ \dot{q} \\ \hline \dot{v} \\ \dot{\phi} \\ \dot{p} \\ \dot{r} \\ \hline \dot{w} \end{bmatrix}
=
\left[\begin{array}{ccc|cccc|c}
X_u & -g & X_q & 0 & 0 & 0 & 0 & 0 \\
0 & 0 & 1 & 0 & 0 & 0 & 0 & 0 \\
M_u & 0 & M_q & 0 & 0 & 0 & 0 & 0 \\
\hline
0 & 0 & 0 & Y_v & g & Y_p & 0 & 0 \\
0 & 0 & 0 & 0 & 0 & 1 & 0 & 0 \\
0 & 0 & 0 & L_v & 0 & L_p & 0 & 0 \\
0 & 0 & 0 & N_v & 0 & 0 & N_r & 0 \\
\hline
0 & 0 & 0 & 0 & 0 & 0 & 0 & Z_w
\end{array}\right]
\begin{bmatrix} u \\ \theta \\ q \\ \hline v \\ \phi \\ p \\ r \\ \hline w \end{bmatrix}
$$

The stability derivatives in these equations are computed from approximate relationships using aircraft physical parameters listed in Appendix C, table 3. Many of these stability derivatives are a function of I_x or I_y which are a function of rotor position in the tip-path plane, ψ. This is because the large contribution of the main rotors to these inertia terms is not a constant value. The development of I_x and I_y is given in Appendix B. The stability derivative values are listed in Appendix C, table 4, and the approximate relationships are as follows (ref. 1):

$$X_u = -[T(da_{1NF}/du) + (dH_{TPP}/du)]/m$$

where

$$
\begin{aligned}
da_{1NF}/du &= a_{1NF}/u = (8\theta_0/3) + 2\lambda \\
dH_{TPP}/du &= \rho\sigma A\Omega R c_{do}/4 \\
\lambda &= -v_i/(\Omega R) \\
v_i &= \text{(see Appendix B)} \\
C_T &= \text{(see Appendix B)} \\
A &= \pi R^2 \\
\sigma &= NC/(\pi R) \\
T &= \text{(see Appendix B)}
\end{aligned}
$$

$$X_q = -[T(da_{1NF}/dq) + dH_{TPP}/dq]/m$$

where

$$
\begin{aligned}
da_{1NF}/dq &= -16/(\gamma\Omega) \\
\gamma &= \rho a C R^4/I_b \\
I_b &= m_r R^2/3 \text{ (inertia of a thin rod)} \\
dH_{TPP}/dq &= -\rho a A\sigma(\Omega R)^2\lambda/(2\gamma\Omega)
\end{aligned}
$$

$$Y_v = X_u$$

$$Y_p = -X_q$$

$$Z_w = -\rho A\Omega R(dC_T/d\bar{w})/m$$

where $dC_T/d\bar{w} = a\sigma/[8 + a\sigma\sqrt{(2/C_T)}/2]$

$L_v = -M_u I_y/I_x$

where I_x = (see Appendix B)
I_y = (see Appendix B)

$L_p = M_q I_y/I_x$

$M_u = [h_R(dH_{TPP}/du + T(da_{1NF}/du)) + dM_s/du]/I_y$

where $dM_s/du = NeR(C.F.)da_{1NF}/du/2$
centrifugal force, lb $C.F. = m_r R\Omega^2/2 + m_t R\Omega^2$

$M_q = [h_R(dH_{TPP}/dq + T(da_{1NF}/dq)) + dM_s/dq]/I_y$

where $dM_s/dq = -8NeR(C.F.)/(\gamma\Omega)$

N_v = 0 (due to lack of directional control mechanism)

N_r = 0 (due to lack of directional control mechanism)

Control System Model

The control system of the Da Vinci II is mathematically described in this section and all assumptions and restrictions are discussed.

Description

The main rotor control surfaces of the Da Vinci II move differentially proportional to the optically sensed height difference of the main rotor tips. The control surface actuators are driven by height difference signals, such that these actuators increase the angle of attack of the control surface corresponding to the lower optical sensor and decrease the angle of attack of the control surface corresponding to the higher sensor. This creates a moment proportional to the measured height difference. The optically sensed height and height-difference signals transmitted to the control surface actuators are considered to be accurate and instantaneous for the purposes of this study. The control surfaces move linearly one degree for each foot of height difference measured (this is discussed further in the Numerical Method section).

Mathematical Development

The mathematical development of this control system utilizes small-angle approximations. It consists of three events described by equations (1) through (10):

1. Determination of optically-sensed height, height difference, and actuator signals.

Optically Sensed Height:

$$h_r = h_o + d_a + d_c - wt - R[\sin\phi \cos\psi - \sin\theta \sin\psi] \tag{1}$$

$$h_l = h_o + d_a + d_c - wt - R[\sin\phi \cos(\psi + \pi) - \sin\theta \sin(\psi + \pi)] \tag{2}$$

Height difference:

$$h_r - h_l = -2R[\phi \cos\psi - \theta \sin\psi] \tag{3}$$

Actuator signals:

$$\delta'_{r,cs} = (h_r - h_l)K_a \tag{4}$$

$$\delta'_{l,cs} = (h_r - h_l)K_b \tag{5}$$

where $\quad K_b = -K_a = \dfrac{1(\text{deg/ft})}{57.3(\text{deg/rad})}$

2. Calculation of the rotational accelerations about the c.g. generated as a function of the resultant control surface lift forces.

Resultant control surface lift forces:

$$F_r = -F_l = -0.5\rho[\Omega(R + l_{cs}/2)]^2 S_{cs} a\, \delta_{r,cs} \tag{6}$$

where $\quad \delta_{r,cs}$ = rate and position limited value of $\delta'_{r,cs}$

The analytical method presented in this report evaluates the control system using $\delta'_{r,cs}$, whereas the numerical method uses $\delta_{r,cs}$. The implications of this will be discussed in the next section.

Generated rotational accelerations:

$$\begin{aligned} \dot{p}_{fb} &= 2F_r(R + l_{cs}/2)\cos\psi/I_x \\ &= K_{c,1}\phi + K_{c,2}\theta \end{aligned} \tag{7}$$

where $\quad K_{c,1} = 2Ra\Omega^2\rho K_a(\cos\psi)^2 S_{cs}(R + l_{cs}/2)^3/I_x$

$\quad\quad K_{c,2} = -2Ra\Omega^2\rho K_a \cos\psi \sin\psi\, S_{cs}(R + l_{cs}/2)^3/I_x$

$$\begin{aligned} \dot{q}_{fb} &= -2F_r(R + l_{cs}/2)\sin\psi/I_y \\ &= K_{d,1}\phi + K_{d,2}\theta \end{aligned} \tag{8}$$

where $K_{d,1} = -2Ra\Omega^2\rho K_a \cos\psi \sin\psi\, S_{cs}(R + l_{cs}/2)^3/I_y$

$$K_{d,2} = 2Ra\Omega^2\rho K_a(\sin\psi)^2 S_{cs}(R + l_{cs}/2)^3/I_y$$

3. Feedback of the generated accelerations to the helicopter body-axis accelerations.

$$\dot{p} = L_v v + L_p p + K_{c,1}\phi + K_{c,2}\theta \tag{9}$$

$$\dot{q} = M_u u + M_q q + K_{d,1}\phi + K_{d,2}\theta \tag{10}$$

The control system is designed to drive the measured height difference to zero by generating a restoring moment and associated acceleration. The restoring moment is only present when height differences are present. Contributions of the control surfaces to thrust and induced velocity are neglected and are discussed in Appendix B.

ANALYSES

The stability characteristics of the Da Vinci II have been studied using analytical and numerical methods. The analytical method entailed development of root locus plots in order to define sources of instability of the unaugmented configuration as well as to determine the effect of the control system on the stability of the Da Vinci II in hover. The numerical method entailed development of a discrete simulation for use as a design tool suitable for determining appropriate control system design specifications (e.g., actuator rate limit, actuator position limit, and control surface area).

The kinematic model previously described is decoupled in the longitudinal, lateral, and vertical axes. However, the introduction of the control system couples the longitudinal and lateral axes. This is because the actuation of the control surfaces can induce accelerations in both roll and pitch when the main rotors are not aligned with the x or y axes.

Wind gust perturbations were used in order to study the response of the unaugmented and augmented configurations under similar conditions. The block diagram given in figure 2 depicts the location at which these perturbations are introduced to the kinematic and control system models. A differential control-surface deflection input has also been depicted in figure 2 as an alternative perturbation to the kinematic and control system models, but this perturbation was not used in this study. It has been depicted for illustrative purposes only. The perturbation gains associated with the differential control surface deflection input are defined by equations (11) and (12).

$$D_\theta = \rho\Omega^2(R + l_{cs}/2)^3 S_{cs} a \sin\psi/I_y \tag{11}$$

$$D_\phi = -\rho\Omega^2(R + l_{cs}/2)^3 S_{cs} a \cos\psi/I_x \tag{12}$$

The resultant mathematical equations and perturbations are as follows:

$$
\left[\begin{array}{c} \dot{u} \\ \dot{\theta} \\ \ddot{\theta} \\ \hline \dot{v} \\ \dot{\phi} \\ \ddot{\phi} \\ \hline \dot{w} \end{array}\right]
=
\left[\begin{array}{ccc|ccc|c}
X_u & -g & X_q & 0 & 0 & 0 & 0 \\
0 & 0 & 1 & 0 & 0 & 0 & 0 \\
M_u & K_{d,2} & M_q & 0 & K_{d,1} & 0 & 0 \\
\hline
0 & 0 & 0 & Y_v & g & Y_p & 0 \\
0 & 0 & 0 & 0 & 0 & 1 & 0 \\
0 & K_{c,2} & 0 & L_v & K_{c,1} & L_p & 0 \\
\hline
0 & 0 & 0 & 0 & 0 & 0 & Z_w
\end{array}\right]
\left[\begin{array}{c} u \\ \theta \\ \dot{\theta} \\ \hline v \\ \phi \\ \dot{\phi} \\ \hline w \end{array}\right]
+
\left[\begin{array}{ccc}
X_u & 0 & 0 \\
0 & 0 & 0 \\
M_u & D_\theta & 0 \\
\hline
0 & 0 & 0 \\
0 & 0 & 0 \\
0 & D_\phi & 0 \\
\hline
0 & 0 & Z_w
\end{array}\right]
\left[\begin{array}{c} u' \\ \delta_{cs,d} \\ w' \end{array}\right]
\qquad (13)
$$

where $\dot{u} = X_u(u + u') - g\theta + X_q\dot{\theta}$

$$\ddot{\theta} = M_u(u + u') + K_{d,2}\theta + M_q\dot{\theta} + K_{d,1}\phi + D_\theta\delta_{cs,d}$$

Analytical Method

Root locus plots were developed based on the kinematics and control system equations describing the Da Vinci II. The goals were to define any instabilities of the unaugmented configuration and study the effects of the control system on the stability of the Da Vinci II in hover.

Characteristic polynomials for the unaugmented and augmented configurations were developed and are based on the use of perturbations as inputs and aircraft states as outputs. The development of the characteristic polynomials is given in Appendix D and associated root locus plots are depicted in figures 3 and 4 (ref. 2) for values of control surface area obtained from the results of the discrete simulation, discussed in the next section.

The plot depicting the augmented configuration was developed using $\delta'_{r,cs}$ (not $\delta_{r,cs}$) in the control system feedback equations previously described. This is because rate and position limits represent nonlinearities in the modeled system which cannot be meaningfully represented by root locus analysis. Therefore, the plot depicted in figure 4 is not truly representative of the actual control system model but does illustrate the stability characteristics of the control system with no rate or position limitations.

The control system has no effect on the stability of the vertical axis and it remains decoupled from the longitudinal and lateral axes. The vertical axis is described by a first-order-lag, and is stable because Z_w is negative, as given by equation (14):

$$\dot{w}(t) = Z_w w(t) + Z_w w'(t)$$

$$\frac{w(s)}{w'(s)} = \frac{Z_w}{s - Z_w} \qquad (14)$$

The longitudinal and lateral axes are decoupled for the unaugmented configuration, and are described by the characteristic polynomials given by equations (15) and (16):

$$1 - M_u \frac{(X_q s - g)}{s(s - X_u)(s - M_q)} = 0 \tag{15}$$

$$1 - L_v \frac{(Y_p s + g)}{s(s - Y_v)(s - L_p)} = 0 \tag{16}$$

The longitudinal and lateral axes are coupled for the augmented configuration, and are described by the characteristic polynomial given by equation (17):

$$1 - \frac{K_{c,2}K_{d,1}(s - X_u)(s - Y_v)}{\{(s - X_u)[s(s - M_q) - K_{d,2}] - M_u(X_q s - g)\}\{(s - Y_v)[s(s - L_p) - K_{c,1}] - L_v(Y_p s + g)\}} = 0 \tag{17}$$

The stability derivatives and control system gains M_q, M_u, L_p, L_v, $K_{c,1}$, $K_{c,2}$, $K_{d,1}$, and $K_{d,2}$ are functions of ψ. Thus, the stability characteristics of the longitudinal and lateral axes vary as a function of ψ, as well.

Root locus plots of the unaugmented configuration of the Da Vinci II are depicted in figure 3 for the longitudinal and lateral axes for values of $\psi = 0°$, 45°, and 90°. Roots corresponding to all other values of ψ vary between the roots at $\psi = 0°$ and $\psi = 90°$. Regardless, for any given value of ψ, two complex poles and one real zero are in the unstable region. The unstable poles correspond to s and $(s - M_q)$ for the longitudinal axis, and s and $(s - L_p)$ for the lateral axis. The exact location of the poles and zeros depicted by the root locus plots in figure 3 are given in table 1.

TABLE 1.- POLES AND ZEROS OF UNAUGMENTED CONFIGURATION

Longitudinal Axis	Lateral Axis
$\psi = 0°$	
Zero : 18.94 Poles : 0.078 ± 1.4i, -12.08 M_u : 0.73	Zero : 18.94 Poles : 0.014 ± 0.59i, -11.86 L_v : -0.13
$\psi = 45°$	
Zero : 18.94 Poles : 0.027 ± 0.79i, -11.97 M_u : 0.23	Zero : 18.94 Poles : 0.027 ± 0.79i, -11.97 L_v : -0.23
$\psi = 90°$	
Zero : 18.94 Poles : 0.014 ± 0.59i, -11.86 Mu : 0.13	Zero : 18.94 Poles : 0.078 ± 1.4i, -12.08 L_v : -0.73

The reason two complex poles are in the unstable region for the longitudinal and lateral axes is because the values of M_q and L_p are very small. This places the poles $(s - M_q)$ and $(s - L_p)$ very close to the origin of each root locus plot, next to a pole at the origin, for values of M_u and L_v equal to zero. The locus of these poles quickly diverge toward the zero in the unstable region as M_u and L_v vary to their actual values. The common denominator in the M_q and L_p terms which make them so small is the Lock Number, γ (ratio of aerodynamic forces to inertial forces), which is the ultimate cause of the instability of the unaugmented configuration for the given values of M_u and L_v.

A root locus plot of the augmented configuration of the Da Vinci II is depicted in figure 4 for values of $\psi = 0°$, 45°, and 90°. Roots corresponding to all values of ψ vary between the roots at $\psi = 0°$ and $\psi = 45°$. Regardless, for any given value of ψ at least two real poles are in the stable region. Additionally, one complex pole pair varies between the unstable and stable regions, becoming stable as ψ approaches 45°, again at 135°, 225°, and so on. Another complex pair remains in the unstable region and moves away from the origin as ψ approaches 45°, again at 135°, 225°, and so on. The exact location of the poles and zeros depicted by the root locus plot in figure 4 are given in table 2.

TABLE 2.- POLES AND ZEROS OF AUGMENTED CONFIGURATION

$\psi = 0°$		
Zeros	:	-11.81, -11.81
Poles	:	-11.81, -12.12
Poles	:	0.014 ±2.32i
Poles	:	0.08 ±1.40i
$K_{c,2}\ K_{d,1}$	:	0
$\psi = 45°$		
Zeros	:	-11.81, -11.81
Poles	:	-11.73, -12.05
Poles	:	1.105 ±2.79i
Poles	:	-1.059 ±2.79i
$K_{c,2}\ K_{d,1}$	:	36.13
$\psi = 90°$		
Zeros	:	-11.81, -11.81
Poles	:	-11.81, -12.12
Poles	:	0.014 ±2.32i
Poles	:	0.08 ±1.40i
$K_{c,2}\ K_{d,1}$	:	0

A close inspection of the root locus plot depicted in figure 4 reveals that at least one of the unstable complex pole pairs remains close (less than or equal to 0.014) to the imaginary axis in the unstable region for $\psi = 0°$, 90°, 180°, and so on. The complex poles closest to the imaginary axis are considered to be dominant if the ratio of the real parts of these poles to the real parts of the next closest poles are greater than five (ref. 5). This is the case for the augmented configuration at $\psi = 0°$, 90°, 180°, and so on because the real parts of the unstable complex poles have a ratio of approximately six to the next closest roots. However, as ψ approaches 45°, 135°, 225°, and so on the dominant unstable complex poles move away from the origin and lose their dominance due to the presence of complex poles in virtually the same location in the stable region. The augmented configuration essentially becomes stable at these values of ψ because of the cancellation effect of the unstable complex poles and the presence of the stable, real poles. The characteristics of the augmented configuration vary from slightly unstable to stable for different values of ψ. This analysis represents the characteristics of the control system with no rate or position limiting.

Numerical Method

A discrete simulation was developed to model the kinematics and control system of the Da Vinci II. A description of this simulation is given in Appendix E. Results of the simulation are given in the form of time histories of the state variables in the presence of the wind gust perturbations described previously.

The control system senses position and produces accelerations ($\dot{p}_{fb}$ and $\dot{q}_{fb}$) through the use of the control surfaces. Rate and position limits are physical constraints of the actuator mechanisms used to change the angle of attack of the control surfaces. The rate and position limits were studied in the discrete simulation because they produced lags and decreased the authority, respectively, of the control surfaces. The goal was to reduce the effectiveness of the control surfaces in responding to differential rotor height so that the accelerations produced would not be extreme thereby creating an unstable system. Correspondingly, caution was used in sizing the limits so that the control surfaces would not produce insufficient accelerations. Control surface area was also varied in the discrete simulation in order to change $K_{c,1}$, $K_{c,2}$, $K_{d,1}$, and $K_{d,2}$, thereby changing the stability characteristics of the augmented configuration as well.

Various combinations of rate limit, position limit, and control surface area values were studied for the control system with a step input of a 5-mph forward velocity wind gust. This was a reasonable disturbance because the intent was simply to excite the augmented configuration with the same perturbation used to induce large, unstable motions from the unaugmented configuration. A lateral-velocity wind gust perturbation would have produced the same results because the configuration is symmetrical and the flight condition is hover.

To quantitatively indicate the effectiveness of the control surface parameter being evaluated, the roll and pitch angle absolute values were summed every cycle through the duration of the perturbation and divided by the sum of the roll and pitch angle absolute values ten seconds later (one rotor revolution after the onset of the perturbation) for the same duration. The ratio is defined below for a step input introduced at $t = 1.25$ sec and lasting 2.5 sec:

$$\frac{\Sigma(|\phi| + |\theta|) \quad (\text{from } t = 1.25 \text{ to } 3.75 \text{ sec})}{\Sigma(|\phi| + |\theta|) \quad (\text{from } t = 11.25 \text{ to } 13.75 \text{ sec})} \tag{18}$$

Values greater than one indicate stability, values equal to one indicate marginal stability, and values less than one indicate instability because, respectively, progressively smaller motion changes as the result of perturbations would make the denominator of the above equation smaller than the numerator; no difference in motion changes would result in the denominator equalling the numerator; and increasingly larger motion changes would make the denominator larger than the numerator. The process used to obtain acceptable rate limit, position limit, and control surface area values was to vary one parameter while the other two were held constant. The value of the parameter yielding the highest ratio was chosen and held constant while one of the other two parameters was varied. This iterative process was repeated several times until a maximum ratio value was obtained. Plots for this process are given in figure 5 for parameter variation about values obtained from the final iteration. The final value for S_{cs} of one control surface is 11.5 ft^2, the final value for the rate limit (R.L.) of each control surface actuator is 0.24 rad/sec, and the final value of the position limit (P.L.) of each control surface is 0.04 rad.

It should be noted that the value of the feedback gain, K_a, was arbitrarily chosen and held constant at -0.01745 rad/ft (-1 deg/ft) for the purposes of this study. This parameter represents the amount of control surface angle of attack obtained per foot of rotor-tip-height difference. Varying K_a is mathematically equivalent to varying the control surface area, as can be seen from the control system equations presented previously. The same responses would have been achieved for different values of S_{cs} and K_a, as long as the product $(R + l_{cs}/2)^3 S_{cs} K_a$ remained equal to -6.57×10^4 ft^4-rad (where $l_{cs} = S_{cs}/C$). The value of this product was used in generating the root locus plot described in the previous section.

Unaugmented time histories are given in figure 6 and augmented time histories without rate and position limiting are given in figure 7. These numerical results agree with the analytical results presented previously. The root locus plots given in figures 3 and 4, and the time histories given in figures 6 and 7, show that the augmented configuration with no rate or position limiting improves the stability characteristics of the Da Vinci II when compared to the unaugmented configuration. Exact correlation between the analytical results and numerical results cannot be determined because the system is nonlinear and the natural frequency and damping of each configuration varies as a function of ψ. Additionally, time histories of the augmented configuration with rate limit and position limit values of 0.24 rad/sec and 0.04 rad, respectively, are given in figure 8.

Perturbations are introduced at $\psi = 45°$ (t = 1.25 s) and last until $\psi = 135°$ (t = 3.75 s). The results depicted in figure 6 show oscillatory instability of the unaugmented configuration. The positions, rates, and accelerations depicted in figures 7 and 8 are substantially less than those depicted in figure 6 and eventually subside to zero. The positions and rates depicted in figure 8 appear fairly well damped, except for the roll rate response, when compared to the positions and rates depicted in figures 6 or 7. However, the maximum roll rate attained never exceeds 10 deg/s and subsides in roughly ten seconds as well. The accelerations depicted in figure 8 do not appear well damped. This behavior is due to the summation of the rotational accelerations produced by the control surfaces ($\dot{p}_{fb}$ and $\dot{q}_{fb}$) with the body axis roational accelerations whenever a differential rotor height is present. The control surfaces are extremely active in the first ten seconds and are sensitive to rotor tip height difference ($h_r - h_l$) even with rate and position limiting. However, the maximum pitch and roll accelerations obtained are no greater than 12 deg/sec^2 and 0.8 ft/sec^2, respectively.

RESULTS

Three conclusions can be drawn from the results of the analyses of the kinematic model and control system, presented in this report. The first conclusion is that the unaugmented configuration is unstable, and this is evidenced by the root locus plots depicted in figure 3 and the time histories depicted in figure 6. The second conclusion is that the control system without rate and position limiting improves the stability characteristics of the Da Vinci II, and is considered slightly stable when compared to the unaugmented configuration, and this is evidenced by the root locus plot depicted in figure 4 and the time histories depicted in figure 7. The third conclusion is that the control system with the stated combination of values of the control system design parameters (K_a, S_{cs}, l_{cs}, rate limit, and position limit) is a stable system. This is evidenced by the time histories depicted in figure 8.

The Da Vinci II is a second generation human-powered helicopter prototype. There is no actual flight test data available to validate the kinematic model which was used to study the control system. Although the results depicted in figure 8 show the control system is able to stabilize the Da Vinci II in hover, these results must be considered preliminary until the kinematic model is validated by comparison with actual flight test data or until proven by flight tests.

REFERENCES

1. Bramwell, A. R. S.: Helicopter Dynamics, Edward Arnold, Ltd., London, 1976.
2. The Mathworks, Inc.: P-C MATLAB, Version 2.2, The Mathworks, Inc., Sherdorn, MA, 1986.
3. Bramwell, A. R. S.: Helicopter Dynamics, Edward Arnold, Ltd., London, 1976, p. 111.
4. Brogran, William L.: Modern Control Theory, Second Ed., Prentice-Hall, Englewood Cliffs, NJ, 1985, p. 368.
5. Dorf, Richard C.: Modern Control Systems, Third Ed., Addison-Wesley Publishing Co., CA, 1980, p. 184.
6. Gerald, Curtis F.: Applied Numerical Analysis, Second Ed., Addison-Wesley Publishing Co., Menlo Park, CA, pp. 260-263.
7. Brogan, William L.: Modern Control Theory, Second Ed., Prentice-Hall, Englewood Cliffs, NJ, 1985, p. 75.

APPENDIX A

AXIS SYSTEMS

The equations describing the kinematics are used to calculate the accelerations about the c.g. of the Da Vinci II. These are body axis accelerations. The body axis system has its origin about the c.g. and is depicted in figure 9.

The equations describing the control system use ground height to calculate control surface deflection. The ground height is referenced relative to the earth. The earth axis reference system used is also depicted in figure 9.

APPENDIX B

SPECIAL CONSIDERATIONS

This appendix contains the analysis and development of mathematical relationships which describe elements of this study which are unique. There are four elements and associated assumptions, as follows:

1. Aeroelasticity: affects the calculation of thrust and mass moment-of-inertias.

2. Tip-losses: reduce the effective rotor radius, however the effect is negligible.

3. Ground effect: affects the calculation of thrust and induced velocity.

4. Control surface contributions to thrust and induced velocity: are considered negligible.

The justification and associated mathematical development for these assumptions are herein described.

The first consideration is aeroelasticity. The Da Vinci II was designed with tension cables to reduce bending of the main rotors in hover. The measured tip deflection and coning angle, β, during a flight test were roughly 12 ft and10°, respectively, and no main rotor pitching or flapping motion was noted. Based on this information the Da Vinci II was modelled using rigid-rotor equations at a constant coning angle of 10°. The inertial representation is depicted in figure 10, and the calculation of the c.g. location, I_x, and I_y are given by equations (19), (20), and (21), as follows:

1. Center-of-gravity calculation:

$$md = 2[m_r(d_a + d_c/2) + m_t(d_a + d_c)] + m_b d_b \tag{19}$$

$$d = 5.5 \text{ feet}$$

2. I_x calculation:

$I_x = 2m_b d_b^2/3 + m_b(d - d_b)^2$
(contribution of pilot and pilot compartment)

$+ 2m_r(R \cos\beta \cos\psi)^2/3 + 2m_r(d_a + d_c/2 - d)^2$
$+ 2m_r(R \cos\beta \sin\psi)^2/12$
(contribution of main rotors)

$+ 2m_t(R \cos\beta \cos\psi)^2 + 2m_t(d_a + d_c - d)^2$
(contribution of mass at rotor tips)

$$I_x = 221.0 + 1133.3 (\sin\psi)^2 + 7253.2 (\cos\psi)^2 \tag{20}$$

3. I_y calculation:

$$I_y = 2m_b d_b^2/3 + m_b(d - d_b)^2$$
(contribution of pilot and pilot compartment)

$$+ 2m_r(R \cos\beta \sin\psi)^2/3 + 2m_r(d_a + d_c/2 - d)^2$$
$$+ 2m_r(R \cos\beta \cos\psi)^2/12$$
(contribution of main rotors)

$$+ 2m_t(R \cos\beta \sin\psi)^2 + 2m_t(d_a + d_c - d)^2$$
(contribution of mass at rotor tips)

$$I_y = 221.0 + 1133.3(\cos\psi)^2 + 7253.2(\sin\psi)^2 \tag{21}$$

Thrust is also affected by aeroelasticity because the resultant lift vector of each rotor is tilted inboard by the amount of the coning angle. The thrust required to hover is calculated by equation (22), as follows:

$$T_\infty = \sqrt{\frac{W^2 + D_o^2}{(\cos\beta)^2}} \tag{22}$$

where $D_o = c_{do}\rho CR(\Omega R)^2 = 8.5$ lb
$W = 285$ lb
$T_\infty = 290.47$ lb

The second consideration is tip losses, which tend to reduce the effective rotor radius. Equation (23) can be used to define the effective rotor radius, as follows (ref. 3):

$$\frac{R_e}{R} = 1 - \frac{\sqrt{C_{T_\infty}}}{N} \tag{23}$$

where $$C_{T_\infty} = \frac{T_\infty}{\rho A(\Omega R)^2}$$

$$C_{T_\infty} = 0.00489$$

For this study equation (23) is modified to account for coning which reduces R_e by $\cos\beta$, and is given by equation (24), as follows:

$$R_e = \left\{\left[1 - \frac{\sqrt{C_{T_\infty}}}{N}\right]R\right\}\cos\beta \tag{24}$$

$$R_e = \{64.66\}\cos\beta = 63.86 \text{ ft}$$

The effective radius, R_e, calculated above constitutes a 4.7% reduction in size of the actual radius, R. Ground effect is estimated to decrease the value of the thrust coefficient by 16.7% as is justified further on in this appendix. This decrease in the thrust coefficient increases R_e to 64.06 ft. Furthermore, the 6-ft diameter, tip-mounted propellers generate an induced velocity component perpendicular to the rotor span, which would tend to increase R_e to an even greater value. Based on all of the above information, it can be seen that R_e approaches the value of R, so tip losses are essentially neglected.

The third consideration is ground effect. It is known that the induced velocity and thrust required to hover are considerably reduced in ground effect. The ratio of induced velocity to that which would have occurred in free air is shown in figure 11 as a function of the radial position and the ratio of rotor height to rotor radius. The ratio of thrust in ground effect to thrust in free air at a given free air power setting as a function of rotor height and thrust coefficient/solidity is also shown in figure 11 (ref. 3). The determination of induced velocity ratio is subject to the assumption that induced velocity is considered to be uniform for the purposes of this study. Induced velocity, v_i, is actually directly proportional to radial location (e.g., $v_i = kr$, from $r = 0$ to $r = R$) such that the average value is located at $r/R = 2/3$. This average value is used as the uniform value, and the induced velocity ratio can be obtained from figure 11 based on $r/R = 2/3$. The rotor height, h, at this location is 22 ft based on the fact that the hovering height of the lowest point of the Da Vinci II, h_o, is 10 ft off the ground. Therefore, $h/r \doteq 0.5$, and the induced velocity ratio, v_i/v_{i_∞}, obtained from figure 11 is approximately 0.35. The determination of thrust ratio is a function of h/r and C_{T_∞}/σ. The value of C_{T_∞}/σ is 0.17 and the thrust ratio at a given free-air power setting obtained from figure 11 is approximately 1.2. The inverse of this value represents the ratio of thrust required to hover in ground effect to thrust required to hover in free air, and is approximately 0.833. This constitutes a 16.7% decrease in the thrust required and the thrust coefficient when in ground effect.

The fourth consideration is the effect of the control surfaces on thrust and induced velocity. The results of this report show that each control surface area should be 11.5 ft^2 in order to obtain a stable, well behaved system. The control surfaces are set at the zero-lift angle of attack when the rotors are leveled or when the control system is off. The control surfaces move differentially when actuated, therefore the total lift generated equals zero at all times. Drag is generated and must be included in the profile drag calculation used above for the development of thrust required to hover and induced velocity. Equation (25) calculates this value of drag, as follows:

$$D = D_o + D_{cs}(max) \tag{25}$$

where

$$D_{cs}(max) = c_{do}\rho[\Omega(R + l_{cs}/2)]^2 S_{cs}$$
$$S_{cs} = 11.5 \text{ ft}^2$$
$$l_{cs} = S_{cs}/C = 3.83 \text{ ft}$$
$$D_{cs}(max) = 0.51 \text{ lb}$$

This value comprises roughly 6.0% of D_o. Based on this information the contributions of the control surfaces to thrust and induced velocity are neglected.

Therefore, the expressions and values for I_x, I_y, T, C_T, and v_i based on aeroelasticity and ground effect for hovering flight are restated by equations (26) to (30), as follows:

$$I_x = 221.0 + 1133.3(\sin\psi)^2 + 7253.2(\cos\psi)^2 \tag{26}$$

$$I_y = 221.0 + 1133.3(\cos\psi)2 + 7253.2(\sin\psi)^2 \tag{27}$$

$$T = 290.47/1.2 = 242.06 \text{ lb} \tag{28}$$

$$C_T = 0.00489/1.2 = 0.00408 \tag{29}$$

$$v_i = 0.35 \times v_{i_\infty} = 0.69 \text{ ft/sec} \tag{30}$$

where $v_{i_\infty} = 2\sqrt{T_\infty/(\rho A)}/3 = 1.96$

APPENDIX C

AIRCRAFT PARAMETER AND DERIVATIVE VALUES

This appendix contains two tables. The first table, table 3, lists values for all aircraft specifications of the Da Vinci II. The second table, table 4, lists values for all stability derivatives, as well as control system parameters used during the course of this study.

TABLE 3.- AIRCRAFT SPECIFICATIONS

Symbol	Value	Symbol	Value
a	6.45	h	22.0
A	14,102.19	h_o	10.0
h_R	1.5	m	8.85
I_b	2323.5	m_b	5.12
β	0.17452	m_r	1.55
C	3.0	m_t	0.31
c_{do}	0.01	Ω	0.6283
C_T	0.00408	N	2
C_{T_∞}	0.00489	σ	0.0285
C.F.	28.75	R	67.0
d	5.5	ρ	0.002378
d_a	4.0	λ	-0.0164
d_b	1.5	θ_o	0.1745
d_c	12.0	W	285.00
d_p	6.0	t_{mr}	0.33
D_o	8.5	T	242.06
e	1.0	T_∞	290.47
γ	399.07	v_i	0.69
g	32.2	v_{i_∞}	1.96

TABLE 4.- STABILITY DERIVATIVES AND CONTROL SYSTEM PARAMETERS

Symbol	Value
S_{cs}	11.5
l_{cs}	3.83
$D_\theta I_x/\sin\psi$	22790.0
$D_\phi I_y/\cos\psi$	-22790.0
K_a	0.017452
K_b	-0.017452
$K_{c,1}I_x/(\cos\psi)^2$	-53296.0
$K_{c,2}I_x/(\sin\psi\cos\psi)$	53296.0
$K_{d,1}I_y/(\sin\psi\cos\psi)$	53296.0
$K_{d,2}I_y/(\sin\psi)^2$	-53296.0
L_pI_x	-149.0
L_vI_x	-988.6
M_qI_y	-149.0
M_uI_y	988.6
N_r	0
N_v	0
X_q	1.70
X_u	-11.81
Y_p	-1.70
Y_v	-11.81
Z_w	-2.92

APPENDIX D

CHARACTERISTIC POLYNOMIAL DEVELOPMENT

The development of the characteristic polynomials for the longitudinal and lateral modes of the unaugmented and augmented configurations of the Da Vinci II are described in this appendix. The equations describing the kinematics and control system were rearranged in state form such that the characteristic polynomials are defined by $\{\det[sI - A]\} = 0$ (ref. 7).

The longitudinal mode of the unaugmented configuration is considered first, as described by equations (31) to (34).

$$\dot{u} = X_u u - g\theta + X_q q + X_u u' \tag{31}$$

$$\dot{q} = M_u u + M_q q + D_\theta \delta_{cs,d} + M_u u' \tag{32}$$

$$\dot{\theta} = q \tag{33}$$

$$\begin{bmatrix} \dot{x}_1 \\ \dot{x}_2 \\ \dot{x}_3 \end{bmatrix} = \begin{bmatrix} X_u & -g & X_q \\ 0 & 0 & 1 \\ M_u & 0 & M_q \end{bmatrix} \begin{bmatrix} x_1 \\ x_2 \\ x_3 \end{bmatrix} + \begin{bmatrix} X_u & 0 \\ 0 & 0 \\ M_u & D_\theta \end{bmatrix} \begin{bmatrix} u' \\ \delta_{cs,d} \end{bmatrix}$$

$$\begin{bmatrix} u \\ \theta \\ \dot{\theta} \end{bmatrix} = \begin{bmatrix} 1 & 0 & 0 \\ 0 & 1 & 0 \\ 0 & 0 & 1 \end{bmatrix} \begin{bmatrix} x_1 \\ x_2 \\ x_3 \end{bmatrix}$$

Solving for $\{\det[sI - A]\} = 0$:

$$\{\det[sI - A]\} = s(s - X_u)(s - M_q) - sM_uX_q + gM_u = 0$$

$$= 1 - M_u \frac{(X_q s - g)}{s(s - X_u)(s - M_q)} = 0 \tag{34}$$

The lateral mode characteristic polynomial of the unaugmented configuration was developed in a similar fashion and is described by equation (35):

$$\{\det[sI - A]\} = s(s - Y_v)(s - L_p) - sL_vY_p + gL_v = 0$$

$$= 1 - L_v \frac{(Y_p s + g)}{s(s - Y_v)(s - L_p)} = 0 \tag{35}$$

The augmented configuration is considered next. The equations describing the kinematics and control system are combined and the longitudinal and lateral modes become coupled, as described by equations (36) to (40), as follows:

$$\dot{u} = X_u u - g\theta + X_q\dot{\theta} + X_u u' \tag{36}$$

$$\ddot{\theta} = M_u u + M_q\dot{\theta} + K_{d,1}\phi + K_{d,2}\theta + D_\theta\delta_{cs,d} + M_u u' \tag{37}$$

$$\dot{v} = Y_v v + g\phi + Y_p\dot{\phi} \tag{38}$$

$$\ddot{\phi} = L_v v + L_p\dot{\phi} + K_{c,1}\phi + K_{c,2}\theta + D_\phi\delta_{cs,d} \tag{39}$$

$$\begin{bmatrix} \dot{x}_1 \\ \dot{x}_2 \\ \dot{x}_3 \\ \dot{x}_4 \\ \dot{x}_5 \\ \dot{x}_6 \end{bmatrix} = \begin{bmatrix} X_u & 0 & -g & X_q & 0 & 0 \\ 0 & Y_v & 0 & 0 & g & Y_p \\ 0 & 0 & 0 & 1 & 0 & 0 \\ M_u & 0 & K_{d,2} & M_q & K_{d,1} & 0 \\ 0 & 0 & 0 & 0 & 0 & 1 \\ 0 & L_v & K_{c,2} & 0 & K_{c,1} & L_p \end{bmatrix} \begin{bmatrix} x_1 \\ x_2 \\ x_3 \\ x_4 \\ x_5 \\ x_6 \end{bmatrix} + \begin{bmatrix} X_u & 0 \\ 0 & 0 \\ 0 & 0 \\ M_u & D_\theta \\ 0 & 0 \\ 0 & D_\phi \end{bmatrix} \begin{bmatrix} u' \\ \delta_{cs,d} \end{bmatrix}$$

$$\begin{bmatrix} x_1 \\ x_2 \\ x_3 \\ x_4 \\ x_5 \\ x_6 \end{bmatrix} = \begin{bmatrix} 1 & 0 & 0 & 0 & 0 & 0 \\ 0 & 1 & 0 & 0 & 0 & 0 \\ 0 & 0 & 1 & 0 & 0 & 0 \\ 0 & 0 & 0 & 1 & 0 & 0 \\ 0 & 0 & 0 & 0 & 1 & 0 \\ 0 & 0 & 0 & 0 & 0 & 1 \end{bmatrix} \begin{bmatrix} u \\ v \\ \theta \\ \dot{\theta} \\ \phi \\ \dot{\phi} \end{bmatrix}$$

Solving for $\{\det[sI - A]\} = 0$ using pivotal condensation (also called the method of Chio) for the augmented configuration yields the following characteristic polynomial (ref. 4):

$$1 - \frac{K_{c,2}K_{d,1}(s - X_u)(s - Y_v)}{\{(s - X_u)[s(s - M_q) - K_{d,2}] - M_u(X_q s - g)\}\{(s - Y_v)[s(s - L_p) - K_{c,1}] - L_v(Y_p s + g)\}} = 0 \tag{40}$$

APPENDIX E

DISCRETE SIMULATION DESCRIPTION

A discrete simulation was developed at the NASA Ames Research Center Flight Systems and Simulation Research Division to study the stability characteristics of the augmented configuration of the Da Vinci II and to size control system design parameters in order to achieve a stable, well behaved system.

The simulation was written in Fortran and was comprised of one main program and four subroutines called by the main program. The main program called the four subroutines in the same order in 12 separate loops. The function of each subroutine and the purpose of the loops are described in this appendix; a flow diagram is shown in figure 12.

The function of the first subroutine is to introduce perturbations to the system of equations describing the kinematic model. The perturbations are in the form of body axis velocity wind gusts, u' and w'. ψ is integrated in this subroutine so that at a particular point in time of a simulation run, a value of u' or w' is introduced. This value is reset back to zero in a finite amount of time so that the input resembles a step.

The function of the second subroutine is to model the control system of the Da Vinci II. This subroutine calculates rotor tip height, rotor tip height difference, control surface deflections, and restoring-moments and associated accelerations ($\dot{p}_{fb}$ and $\dot{q}_{fb}$). The control surface deflection that is calculated from the rotor height difference is differentiated so that a rate limit can be imposed on the system. The rate-limited value is then integrated so that a position limit can be imposed. These two parameters, along with control surface area, were varied in order to define design specifications of the actuators necessary to achieve the desired, stable behavior.

The function of the third subroutine is to model the kinematic equations. This subroutine calculates body axis accelerations and uses Adam's-Bashforth integration to obtain body axis rates and positions (ref. 6). Some of these rates and positions are used by the kinematic model and control system for each successive cycle. The cycle time used for this simulation is 0.05 sec.

The function of the fourth subroutine is to print the aircraft states and stability derivatives of the Da Vinci II. This subroutine prints a line each second stating that the control system is on, if that be the case. Finally, this subroutine will print a "CRASH" message if a rotor hits the ground, and will stop printing after that printout. However, the simulation continues to cycle until the run is complete.

These subroutines are called in 12 separate loops. The first loop initializes arrays and variables in each subroutine as well as the main program. The second loop sets appropriate variables to their trim values for hovering flight. The trim conditions for this simulation are as follows:

$h_o = 10.0$ ft

$\Omega = 0.6283$ rad/sec

Body axis accelerations, rates, and positions are initialized to zero

Variables used in numerical integration and differentiation are initialized to zero

The control system is turned off

The third loop introduces the u' perturbation to the kinematic model and allows the simulation to cycle for 1 min, printing aircraft states and stability derivatives each second. These three loops are repeated using the w' perturbation. The whole process is then repeated with the control system turned on.

The actual Fortran code for this simulation is contained herein. Fortran variables, definitions, and associated units are defined in the Comments sections of the main program and four subroutines. Comments are also included in the code in order to explain the logic.

```
C   TITLE
C
C   PROGRAM COMMAND
C
C-----------------------------------------------------------------------------------------------
C   CREATION/MODIFICATION LOG:
C
C   DATE   NAME              REMARKS
C
C   3/88   J. TOTAH (NASA)   WRITTEN
C-----------------------------------------------------------------------------------------------
C
C   INTRODUCTION:
C   --------------------
C   THIS PROGRAM CONTROLS THE CALLING SEQUENCE OF THE SUBROUTINES
C   THAT COMPRISE THE MODEL FOR THE CALIFORNIA POLYTECHNIC HUMAN-
C   POWERED HELICOPTER PROJECT, THE DAVINCI II.  THE CALLING
C   SEQUENCE IS AS FOLLOWS:
C
C   PROGRAM    SUBROUTINES
C   --------------   -------------------
C   COMMAND -- CHKDYN
C           -- CONTR2
C           -- AERO2
C           -- PRTOUT
C
C   THE SUBROUTINES' FUNCTIONS ARE DEFINED AS FOLLOWS:
C
C   CHKDYN: CALCULATES CONTROL SURFACE PERTURBATIONS
C   CONTR2 : CALCULATES RESTORING MOMENT AND ACCELERATION FEEDBACK
C   AERO2   : CALCULATES AIRCRAFT STATES, BODY AXIS AND EARTH AXIS
C   PRTOUT : PRINTS AIRCRAFT STATES AND STABILITY DERIVATIVES
C
C   DEFINITIONS OF VARIABLES ARE AS FOLLOWS:
C   ---------------------------------------------------------------
C     INPUTS:
C
C ITRIM         IA(06)  NUMBER OF CYCLES TO TRIM                CYC       DATA
C INIT          IA(07)  NUMBER OF CYCLES TO INITIALIZE          CYC       DATA
C ID            IA(05)  SWITCH TO STOP PRTOUT UPON IMPACT       N/A       PRTOUT
C
C RPM           DA(033) ROTOR SPEED                             RAD/SEC   CONTR2
C DT2           DA(088) CYCLE TIME                              SEC       CONTR2
C
C
C     OUTPUTS:
C
C IMODE         IA(01)  MODE CTRL. INT. (-:IC 0:HLD +:OP)       N/A   COMMAND
C IPART         IA(02)  COUNTER USED IN PRTOUT                  N/A   COMMAND
C ICHKDYN       IA(03)  SWITCH TO ACTIVATE 'CHKDYN'             N/A   COMMAND
C ISAS          IA(08)  SWITCH TO TURN SAS ON AND OFF           N/A   COMMAND
C IDEL1         IA(13)  LONGITUDINAL WIND GUST SWITCH           N/A   COMMAND
```

```
C IDEL2          IA(14)  VERTICAL WIND GUST SWITCH                N/A    COMMAND
C
C     LOCALS:
C
C IDYNAMIC IA(04)     NUMBER OF CYCLES FOR 6 REVOLUTION         CYC    COMMAND
C
C
C
         COMMON /DAVINCI/DA(150)
         COMMON /IFIXED/IA(20)
C
C
C
         EQUIVALENCE (IA(01),IMODE          )
         EQUIVALENCE (IA(02),IPART          )
         EQUIVALENCE (IA(03),ICHKDYN        )
         EQUIVALENCE (IA(05),ID             )
         EQUIVALENCE  (IA(08),ISAS          )
         EQUIVALENCE (IA(13),IDEL1          )
         EQUIVALENCE (IA(14),IDEL2          )
C
         EQUIVALENCE (DA(033),RPM           )
         EQUIVALENCE (DA(088),DT2           )
C
C
C
         DATA INIT, ITRIM  /   10 ,  10 /
         DATA DA  , IA     /150*0.,10*0./
C
C**** BEGIN EXECUTABLE CODE
C
         IDYNAMIC = ((12.*3.1415)/RPM) * (1./DT2)
C
C
C
         ISAS = 0
         DO 25 K = 1,2
         IF (K .EQ. 2) ISAS = 1
         IDEL1 = 1
         IDEL2 = 0
         DO 20 J = 1,2
         IF (J .EQ. 2) IDEL1 = 0; IDEL2 = 1
C
C**** CYCLE IN I.C. MODE TO INITIALIZE FILTERS AND VARIABLES
C
         IMODE      = -1
         ICHKDYN  =  0
         IPART      =  0
C
         DO 5 I       = 1,INIT
         IPART       = IPART      + 1
         CALL CHKDYN(I)
         CALL CONTR2
```

```
      CALL AERO2
      CALL PRTOUT
    5  CONTINUE
C
C**** TRIM THE     AIRCRAFT
C
      IMODE      = -1
      ICHKDYN  = 0
      IPART      = 0
C
      DO 10 I       = 1,ITRIM
      IPART       = IPART      + 1
      CALL CHKDYN(I)
      CALL CONTR2
      CALL AERO2
      CALL PRTOUT
   10  CONTINUE
C
C**** PERFORM DYNAMIC CHECKS ON THE AIRCRAFT
C
      IMODE      = 1
      ICHKDYN  = 1
      IPART      = -1
      ID           = 0
C
      DO 15 I      = 1,IDYNAMIC
      IF (ID.EQ.1) GO TO 14
      IPART       = IPART      + 1
      CALL CHKDYN(I)
      CALL CONTR2
      CALL AERO2
      CALL PRTOUT
   14  CONTINUE
   15  CONTINUE
C
   20  CONTINUE
   25  CONTINUE
C
C
C
      STOP
      END
C
C
C  TITLE
C
C  SUBROUTINE CHKDYN
C
      SUBROUTINE  CHKDYN(I)
--------------------------------------------------------------------------------
C
C-------------------------------------------------------------------------------
C  CREATION/MODIFICATION     LOG:
C
```

```
C    DATE    NAME           REMARKS
C
C    3/88    J. TOTAH       (NASA) WRITTEN
C------------------------------------------------------------
C
C    INTRODUCTION:
C    --------------------
C    THIS SUBROUTINE PERTURBS THE SYSTEM WITH LONGITUDINAL AND
C    VERTICAL WIND GUST PERTURBATIONS.
C
C    DEFINITIONS OF VARIABLES ARE AS FOLLOWS:
C    ------------------------------------------------------------
C    INPUTS:
C
C I                      LOOP COUNTER                               N/A   COMMAND
C ICHKDYN IA(04)         SWITCH TO INTRODUCE PERTURBATIONS          N/A   COMMAND
C IDEL1   IA(13)         LONGITUDINAL WIND GUST SWITCH              N/A   COMMAND
C IDEL2   IA(14)         VERTICAL WIND GUST SWITCH                  N/A   COMMAND
C
C GTIME   DA(119)        BEGINNING OF INPUT                         SEC   DATA
C
C    OUTPUTS:
C
C XXI           DA(049)  ROLL MOMENT-OF-INERTIA        SLUGS-FT2     CHKDYN
C YYI           DA(050)  PITCH MOMENT-OF-INERTIA       SLUGS-FT2     CHKDYN
C PSIR          DA(089)  ROTOR POSITION IN THE TPP     RAD           CHKDYN
C DEL1          DA(117)  LONGITUDINAL WIND GUST        FT/2          CHKDYN
C DEL2          DA(118)  VERTICAL WIND GUST            FT/2          CHKDYN
C
C    LOCALS:
C
C NTIME         IA(09)   TIME     TO BEGINNING OF INPUT        CYC   CHKDYN
C NNIME         IA(10)   DURATION OF INPUT                     CYC   CHKDYN
C
C
      COMMON /DAVINCI/DA(150)
      COMMON /IFIXED/IA(20)
C
C
C

      EQUIVALENCE (IA(03),ICHKDYN   )
      EQUIVALENCE (IA(13),IDEL1     )
      EQUIVALENCE (IA(14),IDEL2     )
C
      EQUIVALENCE (DA(028),RADIUS   )
      EQUIVALENCE (DA(032),RHO      )
      EQUIVALENCE (DA(033),RPM      )
      EQUIVALENCE (DA(038),XMASS    )
      EQUIVALENCE (DA(039),XMR      )
      EQUIVALENCE (DA(040),XMB      )
      EQUIVALENCE (DA(041),XMT      )
      EQUIVALENCE (DA(042),BETA     )
      EQUIVALENCE (DA(046),DCLDA    )
```

```
      EQUIVALENCE (DA(049),XXI       )
      EQUIVALENCE (DA(050),YYI       )
      EQUIVALENCE (DA(088),DT2       )
      EQUIVALENCE (DA(089),PSIR      )
      EQUIVALENCE (DA(095),CSAREA    )
      EQUIVALENCE (DA(096),XLCS      )
      EQUIVALENCE (DA(097),CG        )
      EQUIVALENCE (DA(111),AD        )
      EQUIVALENCE (DA(112),BD        )
      EQUIVALENCE (DA(113),CD        )
      EQUIVALENCE (DA(117),DEL1      )
      EQUIVALENCE (DA(118),DEL2      )
C
C
C
      DATA GTIME /   1.25  /
C
C**** INERTIA CALCULATIONS AS A FUNCTION OF PSI
C
      PSIR = PSIR + RPM*DT2
C
      XXI  = XMB*(2.*(BD**2)/3. + ((CG - BD)**2)) +
     1 2.*XMR*(((RADIUS*COS(BETA)*COS(PSIR))**2)/3. + (AD+CD/2.-CG)**2
     2          + ((RADIUS*COS(BETA)*SIN(PSIR))**2)/12.) +
     3 2.*XMT*(((RADIUS*COS(BETA)*COS(PSIR))**2)  + (AD+CD-CG)**2)
C
      YYI  = XMB*(2.*(BD**2)/3. + ((CG - BD)**2)) +
     1 2.*XMR*(((RADIUS*COS(BETA)*SIN(PSIR))**2)/3. + (AD+CD/2.-CG)**2
     2          + ((RADIUS*COS(BETA)*COS(PSIR))**2)/12.) +
     3 2.*XMT*(((RADIUS*COS(BETA)*SIN(PSIR))**2) + (AD+CD-CG)**2)
C
      IF (ICHKDYN .NE. 1) GO TO 10
C
C**** SET TIME OF INPUT AND AMPLITUDE OF STEP PURTURBATIONS
C
      NTIME = GTIME/DT2
      NNIME = NTIME*3.
C
C**** DYNAMIC CHECK
C
      IF (I .LE. NTIME) GO TO 10
      IF (I .GE. NNIME) DEL1 = 0.; DEL2 = 0.; GO TO 10
C
C**** THE VALUE 7.333 FT/S REFERS TO A 5 MPH WIND
C
      DEL1 = IDEL1*7.333
      DEL2 =  IDEL2*7.333
C
   10  CONTINUE
C
C
C
      RETURN
```

```
      END
C
C
C
C   TITLE
C
C   SUBROUTINE CONTR2
C
      SUBROUTINE   CONTR2
C
C-------------------------------------------------------------------------------
C   CREATION/MODIFICATION LOG:
C
C   DATE    NAME       REMARKS
C
C   3/88    J. TOTAH   WRITTEN
C-------------------------------------------------------------------------------
C
C   INTRODUCTION:
C   ---------------------
C   THIS SUBROUTINE CALCULATES DIFFERENTIAL ROTOR HEIGHT, CONTROL
C   SURFACE DEFLECTIONS, AND RESTORING MOMENTS AND ACCELERATIONS.
C
C   DEFINITIONS OF VARIABLES ARE AS FOLLOWS:
C   ------------------------------------------------------------
C    INPUTS:
C
C ISAS      IA(07)    AUGMENTATION ON/OFF SWITCH            N/A         DATA
C
C RADIUS    DA(028)   MAIN ROTOR RADIUS                     FT          DATA
C N         DA(029)   NUMBER OF BLADES                      N/A         DATA
C CHORD     DA(030)   MAIN ROTOR CHORD                      FT          DATA
C CDO       DA(031)   PROFILE DRAG COEFFICIENT              N/A         DATA
C RHO       DA(032)   AIR DENSITY AT SEA LEVEL              SLUGS/FT3   DATA
C RPM       DA(033)   ROTOR SPEED                           FT/SEC      DATA
C WAIT      DA(034)   HELICOPTER TOTAL WEIGHT AT HOVER      LB          DATA
C WROTOR    DA(035)   ROTOR BLADE WEIGHT                    LB          DATA
C WBODY     DA(036)   PILOT AND FRAME WEIGHT                LB          DATA
C WTIP      DA(037)   WEIGHT AT ROTOR TIP                   LB          DATA
C BETA      DA(042)   CONING ANGLE                          RAD         DATA
C GEF1      DA(043)   VI GROUND EFFECT FACTOR               N/A         DATA
C GEF2      DA(044)   THRUST GROUND EFFECT FACTOR           N/A         DATA
C THETO     DA(045)   MAIN ROTOR INITIAL PITCH ANGLE        RAD         DATA
C DCLDA     DA(046)   ROTOR LIFT-CURVE-SLOPE                1/RAD       DATA
C E         DA(047)   HINGE OFFSET                          N/A         DATA
C XXI       DA(049)   ROLL MASS MOMENT-OF-INERTIA           FT2-SLUGS   CHKDYN
C YYI       DA(050)   PITCH MASS MOMENT-OF-INERTIA          FT2-SLUGS   CHKDYN
C G         DA(051)   GRAVITY                               FT/S2       DATA
C THETR     DA(072)   PITCH ANGLE, BODY AXIS                RAD         AERO2
C PHIR      DA(073)   ROLL ANGLE, BODY AXIS                 RAD         AERO2
C DT2       DA(088)   CYCLE TIME                            SEC         DATA
C PSIR      DA(089)   ROTOR POSITION IN THE TPP             RAD         CHKDYN
C CSAREA    DA(095)   CONTROL SURFACE AREA                  FT2         DATA
```

```
C GRL          DA(108)  ACTUATOR RATE LIMIT                  RAD/S     DATA
C GPL          DA(109)  ACTUATOR POSITION LIMIT              RAD       DATA
C GKA          DA(110)  HEIGHT-TO-ANGLE GAIN                 RAD/FT    DATA
C AD           DA(111)  DISTANCE FROM BASE TO HUB            FT        DATA
C BD           DA(112)  DISTANCE FROM BASE TO PILOT CG       FT        DATA
C CD           DA(113)  DISTANCE FROM HUB TO ROTOR TIP       FT        DATA
C PSIRIC       DA(114)  INITIAL ROTOR POSITION IN TPP        RAD       DATA
C DEL1         DA(117)  LONGITUDINAL WIND GUST               FT/S      CHKDYN
C DEL2         DA(118)  VERTICAL WIND GUST                   FT/S      CHKDYN
C
C     OUTPUTS:
C
C PBDFB        DA(093)  ROLL ACCELERATION FEEDBACK           RAD/S2    CONTR2
C QBDFB        DA(094)  PITCH ACCELERATION FEEDBACK          RAD/S2    CONTR2
C
C     LOCALS:
C
C
C XLCS         DA(096)  LENGTH OF CONTROL SURFACE            FT        CONTR2
C CG           DA(097)  HELICOPTER CG                        FT        CONTR2
C HITEA        DA(098)  SIGNAL TO ACTUATOR                   RAD       CONTR2
C DHITE        DA(099)  DIFFERENTIATED ACTUATOR SIGNAL       RAD/S     CONTR2
C HITE         DA(100)  CONTROL SURFACE POSITION             RAD       CONTR2
C RREST        DA(104)  RESTORING FORCE OF CONTROLS          LB        CONTR2
C PM           DA(115)  ROLL MOMENT DUE TO CONTROLS          FT-LB     CONTR2
C QM           DA(116)  PITCH MOMENT DUE TO CONTROLS         FT-LB     CONTR2
C
C
C
      COMMON /IFIXED/IA(20)
      COMMON /DAVINCI/DA(150)
C
C
C
      EQUIVALENCE (IA(01),IMODE      )
      EQUIVALENCE (IA(08),ISAS       )
      EQUIVALENCE (IA(13),IDEL1      )
      EQUIVALENCE (IA(14),IDEL2      )
C
      EQUIVALENCE (DA(028),RADIUS    )
      EQUIVALENCE (DA(029),N         )
      EQUIVALENCE (DA(030),CHORD     )
      EQUIVALENCE (DA(031),CDO       )
      EQUIVALENCE (DA(032),RHO       )
      EQUIVALENCE (DA(033),RPM       )
      EQUIVALENCE (DA(034),WAIT      )
      EQUIVALENCE (DA(038),XMASS     )
      EQUIVALENCE (DA(039),XMR       )
      EQUIVALENCE (DA(040),XMB       )
      EQUIVALENCE (DA(041),XMT       )
      EQUIVALENCE (DA(042),BETA      )
      EQUIVALENCE (DA(043),GEF1      )
      EQUIVALENCE (DA(044),GEF2      )
```

```
      EQUIVALENCE (DA(045),THETO    )
      EQUIVALENCE (DA(046),DCLDA    )
      EQUIVALENCE (DA(047),E        )
      EQUIVALENCE (DA(048),HR       )
      EQUIVALENCE (DA(049),XXI      )
      EQUIVALENCE (DA(050),YYI      )
      EQUIVALENCE (DA(051),G        )
      EQUIVALENCE (DA(072),THETR    )
      EQUIVALENCE (DA(073),PHIR     )
      EQUIVALENCE (DA(088),DT2      )
      EQUIVALENCE (DA(089),PSIR     )
      EQUIVALENCE (DA(093),PBDFB    )
      EQUIVALENCE (DA(094),QBDFB    )
      EQUIVALENCE (DA(095),CSAREA   )
      EQUIVALENCE (DA(096),XLCS     )
      EQUIVALENCE (DA(097),CG       )
      EQUIVALENCE (DA(100),HITE     )
      EQUIVALENCE (DA(111),AD       )
      EQUIVALENCE (DA(112),BD       )
      EQUIVALENCE (DA(113),CD       )
      EQUIVALENCE (DA(117),DEL1     )
      EQUIVALENCE (DA(118),DEL2     )
C
C
C
      DATA CDO     , N       / 0.01       , 2        /
      DATA E       , GEF1    / 1.0        , 0.35     /
      DATA THETO   , GEF2    / 0.1745     , 1.2      /
      DATA PSIRIC  , GKA     / -0.031415  , -0.01745 /
      DATA WBODY   , WROTOR  /165.0       , 50.0     /
      DATA WTIP    , WAIT    / 10.0       ,285.0     /
      DATA DCLDA   , RADIUS  / 6.45       , 67.0     /
      DATA CSAREA  , RPM     / 11.5       , 0.6283   /
      DATA DT2  ,    RHO     / 0.05       , 0.002378 /
      DATA G       , AD      / 32.2       , 4.0      /
      DATA BD      , CD      / 1.5        ,12.0      /
      DATA GPL     , GRL     / 0.04       , 0.24     /
      DATA ISAS    , CHORD   / 0          , 3.0      /
      DATA BETA              / 0.1745/
C
C---------------------------------------- IC MODE ----------------------------------------------
C
      IF (IMODE) 100,300,200
C
  100 CONTINUE
C
C**** FILTER INITIALIZATION
C
      PSIR     = PSIRIC
C
      HITEA    = 0.
      HITEAP   = 0.
C
```

```
      HITE      = 0.
      DHITE     = 0.
      DHITEP    = DHITE
C
C**** DESIGN SPECIFICATION CALCULATIONS
C
      XLCS      = SQRT(CSAREA)
      XMB       = WBODY / G
      XMR       = WROTOR/ G
      XMT       = WTIP  / G
      XMASS     = WAIT  / G
      CG        = 2.*(XMR*(AD+CD/2.) + XMT*(AD+CD))/XMASS    +
     1            XMB*BD/XMASS
      HR        = ABS(CG-AD)
C
C------------------------------------- OPERATE MODE ---------------------------------------------
C
 200  CONTINUE
C
C**** CALCULATION OF DIFFERENTIAL ROTOR HEIGHT COMMAND TO ACTUATORS
C
      HITEA     =  2.*RADIUS*(PHIR*COS(PSIR) - THETR*SIN(PSIR))*GKA
     1     *ISAS
C
C**** RATE AND POSITION LIMIT CALCULATIONS
C
      DHITE     = (HITEA - HITEAP)/DT2
      HITEAP    = HITEA
      IF (ABS(DHITE) .GE. GRL)  DHITE = SIGN(GRL,DHITE)
C
      HITE      = HITE + 0.5*DT2*(3.*DHITE - DHITEP)
      DHITEP    = DHITE
C
      IF (ABS(HITE) .GE. GPL)   HITE = SIGN(GPL,HITE)
C
C**** CALC. OF FEEDBACK ACCELERATIONS FROM CONTROL SURFACE DEFLECTIONS
C
      RREST     = DCLDA*HITE*RHO*((RPM*(RADIUS+XLCS/2.))**2.)*CSAREA
C
      QM        =  -RREST*(RADIUS+XLCS/2.)*(SIN(PSIR))
      PM        =   RREST*(RADIUS+XLCS/2.)*(COS(PSIR))
C
      QBDFB     =  IDEL1*QM/YYI
      PBDFB     =  IDEL1*PM/XXI
C
C
C
 300  CONTINUE
C
      RETURN
      END
C
C
```

```
C
C   TITLE
C
C   SUBROUTINE AERO2
C
C
        SUBROUTINE  AERO2
C
C-----------------------------------------------------------------------------------------------
C   CREATION/MODIFICATION LOG:
C
C   DATE    NAME        REMARKS
C
C   3/88    J. TOTAH    WRITTEN
C-----------------------------------------------------------------------------------------------
C
C   INTRODUCTION:
C   ---------------------
C   THIS SUBROUTINE CALCULATES BODY AXIS ACCELERATIONS, FORCES, AND
C   MOMENTS USING CONTROL SURFACE INPUTS FROM CONTR2.
C
C   DEFINITIONS OF VARIABLES ARE AS FOLLOWS:
C   ----------------------------------------------------------
C     INPUTS:
C
C PBDFB     DA(093)   ROLL ACCELERATION FEEDBACK                          CONTR2
C QBDFB     DA(094)   PITCH ACCELERATION FEEDBACK                         CONTR2
C
C     OUTPUTS:
C
C SDXU      DA(001)  LONG. DRAG DAMPING                     RAD/SEC       AERO2
C SDZW      DA(002)  VERTICAL DAMPING                       RAD/SEC       AERO2
C SDMU      DA(003)  LONGITUDINAL VELOCITY STABILITY        RAD/SEC/FT    AERO2
C SDMQ      DA(004)  PITCH DAMPING                          1/RAD/SEC     AERO2
C SDXQ      DA(005)  PARTIAL X-FORCE WRT PITCH RATE         FT/SEC/RAD    AERO2
C SDYV      DA(006)  LATERAL DRAG DAMPING                   RAD/SEC       AERO2
C SDYP      DA(007)  PARTIAL Y-FORCE WRT ROLL RATE          FT/SEC/RAD    AERO2
C SDLV      DA(008)  LATERAL VELOCITY STABILITY             RAD/S/FT      AERO2
C SDLP      DA(009)  ROLL DAMPING                           1/RAD/SEC     AERO2
C UBD       DA(052)  FORWARD  ACCELERATION         BODY  AXIS R/S2      AERO2
C VBD       DA(053)  SIDE    ACCELERATION          BODY  AXIS FT/S2     AERO2
C WBD       DA(054)  VERTICAL ACCELERATION         BODY  AXIS FT/S2     AERO2
C PBD       DA(055)  ROLL    ACCELERATION          BODY  AXIS R/S2      AERO2
C QBD       DA(056)  PITCH   ACCELERATION          BODY  AXIS R/S2      AERO2
C UB        DA(057)  FWD BODY VELOCITY             BODY  AXIS FT/S      AERO2
C VB        DA(058)  LFT BODY VELOCITY             BODY  AXIS FT/S      AERO2
C WB        DA(059)  DWN BODY VELOCITY             BODY  AXIS FT/S      AERO2
C PB        DA(060)  ROLL RATE                     BODY  AXIS RAD/S     AERO2
C QB        DA(061)  PITCH RATE                    BODY  AXIS RAD/S     AERO2
C THETR     DA(072)  PITCH ANGLE                   BODY  AXIS RAD       AERO2
C PHIR      DA(073)  ROLL ANGLE                    BODY  AXIS RAD       AERO2
C XE        DA(080)  LONGITUDINAL POSITION         EARTH AXIS FT        AERO2
C YE        DA(081)  LATERAL POSITION              EARTH AXIS FT        AERO2
```

```
C ZE        DA(082)  VERTICAL POSITION                   EARTH  AXIS FT         AERO2
C FTX       DA(083)  AERODYNAMIC X-FORCE                 BODY   AXIS LBF        AERO2
C FTY       DA(084)  AERODYNAMIC SIDE FORCE              BODY   AXIS LBF        AERO2
C FTZ       DA(085)  AERODYNAMIC VERTICAL FORCE          BODY   AXIS LBF        AERO2
C TTL       DA(086)  AERODYNAMIC ROLL MOMENT             BODY   AXIS FT-LBF     AERO2
C TTM       DA(087)  AERODYNAMIC PITCH MOMENT            BODY   AXIS FT-LBF     AERO2
C
C     LOCALS:
C
C DADU      DA(010)  FLAPPING COEFF. FORCE DUE TO UB      RAD-SEC/FT            AERO2
C DHDU      DA(011)  HUB FORCE DUE TO UB                  SLUGS-RAD/S           AERO2
C DADQ      DA(012)  FLAPPING COEFF. FORCE DUE TO QB      SEC/RAD               AERO2
C DHDQ      DA(013)  HUB FORCE DUE TO QB                  SLUGS-FT/S/RAD        AERO2
C DCTDW     DA(014)  THRUST COEFFICIENT DUE TO WB         N/A                   AERO2
C DMDU      DA(015)  SHAFT MOMENT DUE TO UB               SLUGS-FT-RAD/S        AERO2
C DMDQ      DA(016)                                       N/A                   AERO2
C BBI       DA(024)  ROTOR BLADE INERTIA                  FT2-SLUGS             AERO2
C GLOCH     DA(025)  LOCH NUMBER                          N/A                   AERO2
C CT        DA(026)  COEFFICIENT OF THRUST                N/A                   AERO2
C CF        DA(027)  CENTRIFUGAL FORCE                    LB                    AERO2
C XED       DA(074)  LONGITUDINAL SPEED          EARTH  AXIS FT/S               AERO2
C YED       DA(075)  LATERAL SPEED               EARTH  AXIS FT/S               AERO2
C ZED       DA(076)  VERTICAL SPEED              EARTH  AXIS FT/S               AERO2
C
C
C
      COMMON  /IFIXED/IA(20)
      COMMON  /DAVINCI/DA(150)
C
C
C
      EQUIVALENCE  (IA(001),IMODE        )
C
      EQUIVALENCE  (DA(001),SDXU         )
      EQUIVALENCE  (DA(002),SDZW         )
      EQUIVALENCE  (DA(003),SDMU         )
      EQUIVALENCE  (DA(004),SDMQ         )
      EQUIVALENCE  (DA(005),SDXQ         )
      EQUIVALENCE  (DA(006),SDYV         )
      EQUIVALENCE  (DA(007),SDYP         )
      EQUIVALENCE  (DA(008),SDLV         )
      EQUIVALENCE  (DA(009),SDLP         )
      EQUIVALENCE  (DA(028),RADIUS       )
      EQUIVALENCE  (DA(029),N            )
      EQUIVALENCE  (DA(030),CHORD        )
      EQUIVALENCE  (DA(031),CDO          )
      EQUIVALENCE  (DA(032),RHO          )
      EQUIVALENCE  (DA(033),RPM          )
      EQUIVALENCE  (DA(034),WAIT         )
      EQUIVALENCE  (DA(038),XMASS        )
      EQUIVALENCE  (DA(039),XMR          )
      EQUIVALENCE  (DA(040),XMB          )
      EQUIVALENCE  (DA(041),XMT          )
```

```
      EQUIVALENCE (DA(042),BETA       )
      EQUIVALENCE (DA(043),GEF1       )
      EQUIVALENCE (DA(044),GEF2       )
      EQUIVALENCE (DA(045),THETO      )
      EQUIVALENCE (DA(046),DCLDA      )
      EQUIVALENCE (DA(047),E          )
      EQUIVALENCE (DA(048),HR         )
      EQUIVALENCE (DA(049),XXI        )
      EQUIVALENCE (DA(050),YYI        )
      EQUIVALENCE (DA(051),G          )
      EQUIVALENCE (DA(052),UBD        )
      EQUIVALENCE (DA(053),VBD        )
      EQUIVALENCE (DA(054),WBD        )
      EQUIVALENCE (DA(055),PBD        )
      EQUIVALENCE (DA(056),QBD        )
      EQUIVALENCE (DA(057),UB         )
      EQUIVALENCE (DA(058),VB         )
      EQUIVALENCE (DA(059),WB         )
      EQUIVALENCE (DA(060),PB         )
      EQUIVALENCE (DA(061),QB         )
      EQUIVALENCE (DA(072),THETR      )
      EQUIVALENCE (DA(073),PHIR       )
      EQUIVALENCE (DA(080),XE         )
      EQUIVALENCE (DA(081),YE         )
      EQUIVALENCE (DA(082),ZE         )
      EQUIVALENCE (DA(083),FTX        )
      EQUIVALENCE (DA(084),FTY        )
      EQUIVALENCE (DA(085),FTZ        )
      EQUIVALENCE (DA(086),TTL        )
      EQUIVALENCE (DA(087),TTM        )
      EQUIVALENCE (DA(088),DT2        )
      EQUIVALENCE (DA(089),PSIR       )
      EQUIVALENCE (DA(093),PBDFB      )
      EQUIVALENCE (DA(094),QBDFB      )
      EQUIVALENCE (DA(117),DEL1       )
      EQUIVALENCE (DA(118),DEL2       )
      EQUIVALENCE (DA(123),HO         )
C
C--------------------------------------- IC MODE -------------------------------------------
C
      IF (IMODE) 100,300,200
C
 100  CONTINUE
C
C**** FILTER INITIALIZATIONS
C
      UBD   = 0.
      VBD   = 0.
      WBD   = 0.
      PBD   = 0.
      PB    = 0.
      QBD   = 0.
      QB    = 0.
```

```
C
      UBDP   = UBD
      VBDP   = VBD
      WBDP   = WBD
      PBDP   = PBD
      PBP    = PB
      QBDP   = QBD
      QBP    = QB
C
      UB     = 0.
      WB     = 0.
      VB     = 0.
      PB     = 0.
      PHIR   = 0.
      QB     = 0.
      THETR  = 0.
C
      XED    = 0.
      YED    = 0.
      ZED    = 0.
C
      XEDP   = XED
      YEDP   = YED
      ZEDP   = ZED
C
      XE     = 0.
      YE     = 0.
      ZE     = HO
C
C**** STABILITY DERIVATIVE CALCULATIONS
C
      AREA     =  3.1415*(RADIUS**2)
      SIGMA    =  N*CHORD/(3.1415*RADIUS)
      DO       =  CDO*RHO*CHORD*RADIUS*((RPM*RADIUS)**2)
      TOO      =  SQRT(WAIT**2 + DO**2)/COS(BETA)
      THRUST   =  TOO/GEF2
      VI       =  GEF1*2.*SQRT(TOO/(RHO*AREA))/3.
      XIN      = -VI/(RPM*RADIUS)
C
      DADU     =  8.*THETO/3. + 2.*XIN
      DHDU     =  RHO*SIGMA*AREA*RPM*RADIUS*CDO/4.
C
      SDXU     = -(THRUST*DADU + DHDU)/XMASS
C
C
C
      BBI      =  XMR*(RADIUS**2)/3.
      GLOCH    =  RHO*DCLDA*CHORD*(RADIUS**4)/BBI
C
      DADQ     = -16./(GLOCH*RPM)
      DHDQ     = -RHO*DCLDA*AREA*SIGMA*((RPM*RADIUS)**2)*XIN/
     1            (2.*GLOCH*RPM)
C
```

```
      SDXQ     = -(THRUST*DADQ + DHDQ)/XMASS
C
C
C
      SDYV     =  SDXU
C
C
C
      SDYP     = -SDXQ
C
C
C
      CT       =  TOO/(RHO*AREA*((RPM*RADIUS)**2))/GEF2
      DCTDW    =  DCLDA*SIGMA/(8. + DCLDA*SIGMA*SQRT(2./CT)/2.)
C
      SDZW     = -RHO*AREA*RPM*RADIUS*DCTDW/XMASS
C
C
C
      CF       =  (XMR/2. + XMT)*RADIUS*(RPM**2)
      DMDU     =  N*E*RADIUS*CF*DADU/2.
C
      SDMU     =  (HR*(DHDU + THRUST*DADU) + DMDU)/YYI
C
C
C
      DMDQ     = -8.*N*E*RADIUS*CF/(GLOCH*RPM)
C
      SDMQ     =  (HR*(DHDQ + THRUST*DADQ) + DMDQ)/YYI
C
C
C
      SDLV     = -SDMU*YYI/XXI
C
C
C
      SDLP     =  SDMQ*YYI/XXI
C
C---------------------------------------- OPERATE MODE --------------------------------------------
C
  200    CONTINUE
C
C**** STABILITY DERIVATIVES AS A FUNCTION OF INERTIA (AND PSI)
C
      SDMU   =  (HR*(DHDU + THRUST*DADU) + DMDU)/YYI
      SDMQ   =  (HR*(DHDQ + THRUST*DADQ) + DMDQ)/YYI
      SDLV   = -SDMU*YYI/XXI
      SDLP   =  SDMQ*YYI/XXI
C
C**** STATE MODEL
C
      UBD    =  (UB+DEL1)*SDXU + QB*SDXQ - G*THETR
      WBD    =  (WB+DEL2)*SDZW
```

```
      QBD    = (UB+DEL1)*SDMU + QB*SDMQ + QBDFB
      VBD    = VB*SDYV + PB*SDYP + G*PHIR
      PBD    = VB*SDLV + PB*SDLP + PBDFB
C
      UB     = UB   + 0.5*DT2*(3.*UBD - UBDP)
      WB     = WB   + 0.5*DT2*(3.*WBD - WBDP)
      QB     = QB   + 0.5*DT2*(3.*QBD - QBDP)
      THETR  = THETR+ 0.5*DT2*(3.*QB  - QBP)
      VB     = VB   + 0.5*DT2*(3.*VBD - VBDP)
      PB     = PB   + 0.5*DT2*(3.*PBD - PBDP)
      PHIR   = PHIR + 0.5*DT2*(3.*PB  - PBP)
C
      UBDP   = UBD
      WBDP   = WBD
      QBDP   = QBD
      QBP    = QB
      VBDP   = VBD
      PBDP   = PBD
      PBP    = PB
C
C**** CG RATES AND POSITIONS RELATIVE TO THE EARTH
C
      XED    = UB*COS(THETR) + VB*SIN(PHIR)*SIN(THETR) +
     1         WB*COS(PHIR)*SIN(THETR)
      YED    = VB*COS(PHIR)  - WB*SIN(PHIR)
      ZED    = -UB*SIN(THETR) + VB*SIN(PHIR)*COS(THETR) +
     1         WB*COS(PHIR)*COS(THETR)
C
      XE     = XE + 0.5*DT2*(3.*XED - XEDP)
      YE     = YE + 0.5*DT2*(3.*YED - YEDP)
      ZE     = ZE + 0.5*DT2*(3.*ZED - ZEDP)
C
      XEDP   = XED
      YEDP   = YED
      ZEDP   = ZED
C
C**** AERODYNAMIC FORCE AND MOMENT CALCULATIONS, BODY AXIS
C
      FTX    = UBD*XMASS
      FTY    = VBD*XMASS
      FTZ    = WBD*XMASS
      TTL    = PBD*XXI
      TTM    = QBD*YYI
C
  300 CONTINUE
C
      RETURN
      END
C
C
C
C   TITLE
C
```

```
C    SUBROUTINE PRTOUT
C
          SUBROUTINE  PRTOUT
C
C------------------------------------------------------------------------------------------
C    CREATION/MODIFICATION LOG:
C
C    DATE    NAME                REMARKS
C
C    3/88    J. TOTAH (NASA)     WRITTEN
C------------------------------------------------------------------------------------------
C
C    INTRODUCTION:
C    --------------------
C    THIS SUBROUTINE PRINTS OUT AIRCRAFT STATES AND STABILITY
C    DERIVATIVES EVERY SECOND.
C
C    DEFINITIONS OF VARIABLES ARE AS FOLLOWS:
C    ---------------------------------------------------------
C
C IB         IA(11)  BIAS USED IN PRINTING EVERY SECOND        N/A    PRTOUT
C IPRT       IA(12)  PRINT FLAG                                N/A    PRTOUT
C
C
C HO         DA(085) INITIAL DISTANCE FROM THE GROUND          FT     DATAUT
C TIME       DA(086) TIME IN OPERATE                           SEC    PRTOUT
C XTHET      DA(087) PITCH ANGLE, BODY AXIS                    DEG    PRTOUT
C XPHI       DA(085) ROLL ANGLE, BODY AXIS                     DEG    PRTOUT
C XPSI       DA(086) POSITION OF ROTORS IN TPP                 DEG    PRTOUT
C HITEL      DA(086) HEIGHT OF ROTOR INITIALLY AT 180DEG       FT     PRTOUT
C HITER      DA(087) HEIGHT OF ROTOR INITIALLY AT  90DEG       FT     PRTOUT
C
C
C
        COMMON  /IFIXED/IA(20)
        COMMON  /DAVINCI/DA(150)
C
C
C
        EQUIVALENCE  (IA(01),IMODE          )
        EQUIVALENCE  (IA(02),IPART          )
        EQUIVALENCE  (IA(03),ICHKDYN        )
        EQUIVALENCE  (IA(05),ID             )
        EQUIVALENCE  (IA(08),ISAS           )
C
        EQUIVALENCE  (DA(001),SDXU          )
        EQUIVALENCE  (DA(002),SDZW          )
        EQUIVALENCE  (DA(003),SDMU          )
        EQUIVALENCE  (DA(004),SDMQ          )
        EQUIVALENCE  (DA(005),SDXQ          )
        EQUIVALENCE  (DA(006),SDYV          )
        EQUIVALENCE  (DA(007),SDYP          )
        EQUIVALENCE  (DA(008),SDLV          )
```

```
      EQUIVALENCE  (DA(009),SDLP          )
      EQUIVALENCE  (DA(028),RADIUS        )
      EQUIVALENCE  (DA(052),UBD           )
      EQUIVALENCE  (DA(053),VBD           )
      EQUIVALENCE  (DA(054),WBD           )
      EQUIVALENCE  (DA(055),PBD           )
      EQUIVALENCE  (DA(056),QBD           )
      EQUIVALENCE  (DA(057),UB            )
      EQUIVALENCE  (DA(058),VB            )
      EQUIVALENCE  (DA(059),WB            )
      EQUIVALENCE  (DA(060),PB            )
      EQUIVALENCE  (DA(061),QB            )
      EQUIVALENCE  (DA(072),THETR         )
      EQUIVALENCE  (DA(073),PHIR          )
      EQUIVALENCE  (DA(080),XE            )
      EQUIVALENCE  (DA(081),YE            )
      EQUIVALENCE  (DA(082),ZE            )
      EQUIVALENCE  (DA(083),FTX           )
      EQUIVALENCE  (DA(084),FTY           )
      EQUIVALENCE  (DA(085),FTZ           )
      EQUIVALENCE  (DA(086),TTL           )
      EQUIVALENCE  (DA(087),TTM           )
      EQUIVALENCE  (DA(088),DT2           )
      EQUIVALENCE  (DA(089),PSIR          )
      EQUIVALENCE  (DA(100),HITE          )
      EQUIVALENCE  (DA(111),AD            )
      EQUIVALENCE  (DA(113),CD            )
      EQUIVALENCE  (DA(117),DEL1          )
      EQUIVALENCE  (DA(118),DEL2          )
      EQUIVALENCE  (DA(123),HO            )
C
C
C
      DATA HO / 10. /
C
C**** CODE TO PRINT EACH SECOND
C
      XPSI    =  PSIR*57.3
      XPHI    =  PHIR*57.3
      XTHET   = THETR*57.3
      HITEL   =  AD+CD+ZE+RADIUS*(PHIR*COS(PSIR)-THETR*SIN(PSIR))
      HITER   =  AD+CD+ZE-RADIUS*(PHIR*COS(PSIR)-THETR*SIN(PSIR))
C
      IF (IMODE .EQ. -1) IB = 1; TIME = -DT2*2.
      TIME    = TIME + DT2
      IPRT    = ABS(INT(DT2*IPART) - IB)
      IF (IPRT .EQ. 1 .AND. ICHKDYN .EQ. 1) GO TO 10
      IF (IPRT .EQ. 0) GO TO 10
      GO TO 20
   10   CONTINUE
        IB = IB + 1
C
C**** WRITE STATEMENTS
```

```
C
         WRITE (3,100) TIME
         WRITE (3,110) FTX, UBD, UB, XE   , XTHET
         WRITE (3,120) FTY, VBD, VB, YE   , XPHI
         WRITE (3,130) FTZ, WBD, WB, ZE   , HITE
         WRITE (3,140) TTL, PBD, PB, DEL1 , HITEL
         WRITE (3,150) TTM, QBD, QB, DEL2 , HITER
         WRITE (3,160) XPSI
         WRITE (3,170) SDXU, SDMU, SDYV, SDLV
         WRITE (3,180) SDXQ, SDMQ, SDYP, SDLP
         WRITE (3,190) SDZW
C
         IF  (ISAS .NE. 0) WRITE (3,200)
         IF (HITER .LT. 0 .OR. HITEL .LT. 0) ID = 1; WRITE (3,210)
C
   20    CONTINUE
C
  100    FORMAT(////20X,'AIRCRAFT STATES AT ',F5.2,' SEC',/)
  110    FORMAT('FTX=',F7.2,'       UBD=',F7.2,'    UB=',F7.2,'         XE=',F7.2,
     1      ' XTHET=',F7.2)
  120    FORMAT('FTY=',F7.2,'       VBD=',F7.2,'    VB=',F7.2,'         YE=',F7.2,
     1      '  XPHI=',F7.2)
  130    FORMAT('FTZ=',F7.2,'       WBD=',F7.2,'    WB=',F7.2,'         ZE=',F7.2,
     1      '  HITE=',F7.2)
  140    FORMAT('TTL=',F7.2,'       PBD=',F7.2,'    PB=',F7.2,'     XDEL1=',F7.2,
     1      ' HITEL=',F7.2)
  150    FORMAT('TTM=',F7.2,'       QBD=',F7.2,'    QB=',F7.2,'     XDEL2=',F7.2,
     1      ' HITER=',F7.2)
  160    FORMAT(//15X,'AIRCRAFT STABILITY DERIVATIVES AT PSI = ',F7.2,/)
  170    FORMAT('SDXU=',F9.2,'  SDMU=',F9.2,'  SDYV',F9.2,'  SDLV=',F9.2)
  180    FORMAT('SDXQ=',F9.2,'  SDMQ=',F9.2,'  SDYP',F9.2,'  SDLP=',F9.2)
  190    FORMAT('SDZW=',F9.2)
  200    FORMAT(/20X,'THE CONFIGURATION IS AUGMENTED')
  210    FORMAT(10X,'******************** CRASH ********************')
C
C
C
         RETURN
         END
```

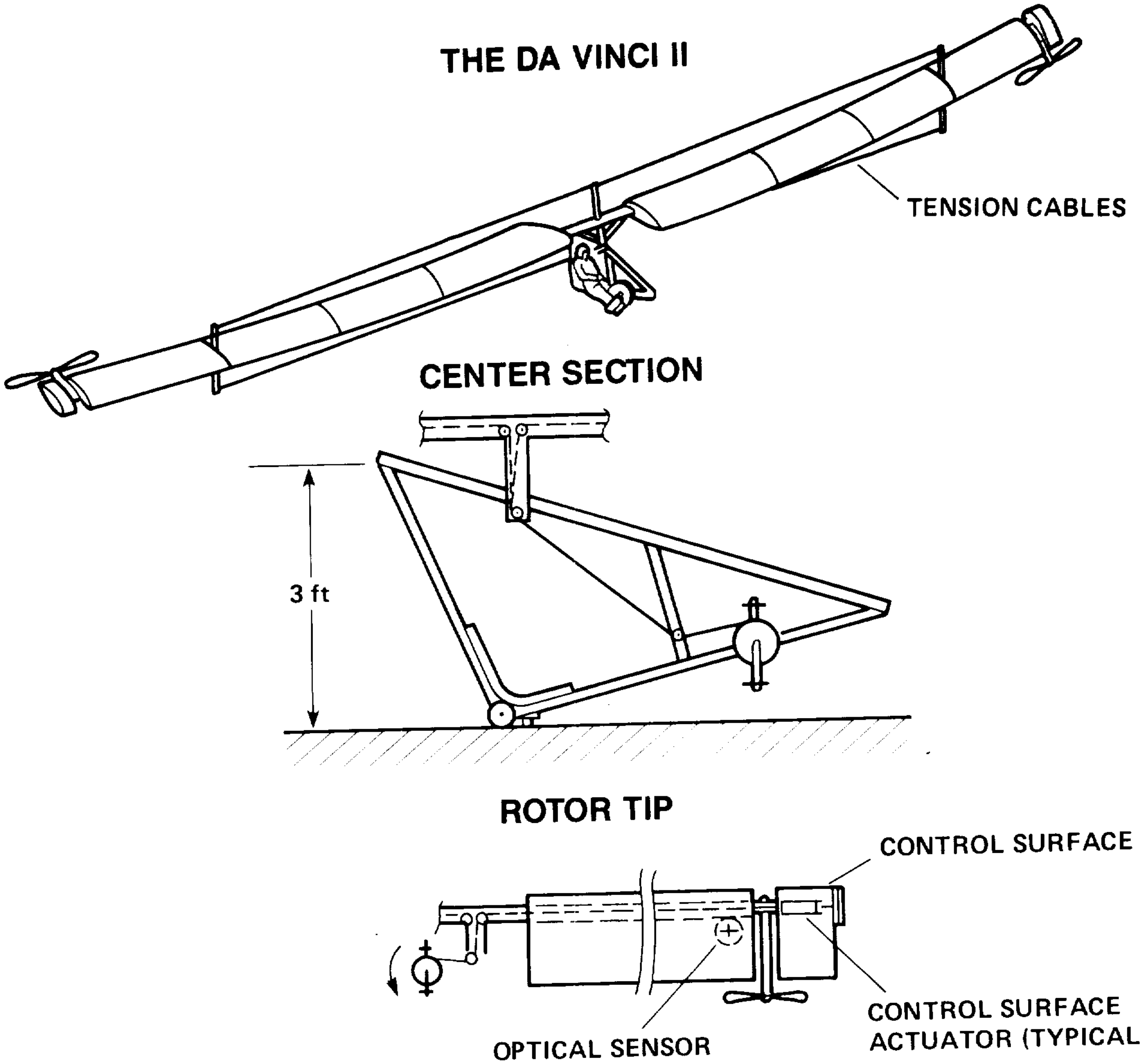

Figure 1.- Aircraft description.

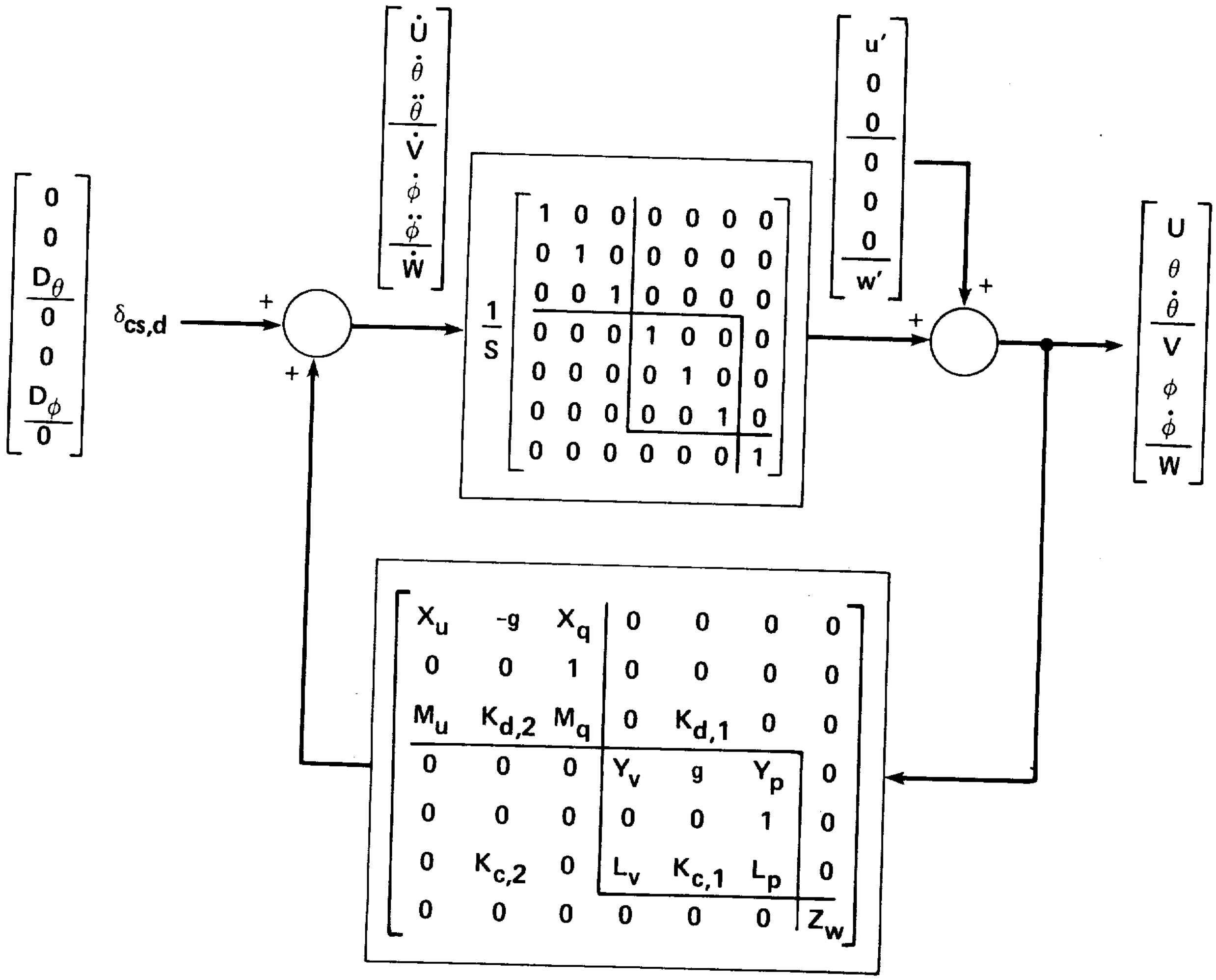

Figure 2.- Kinematic and control system block diagram.

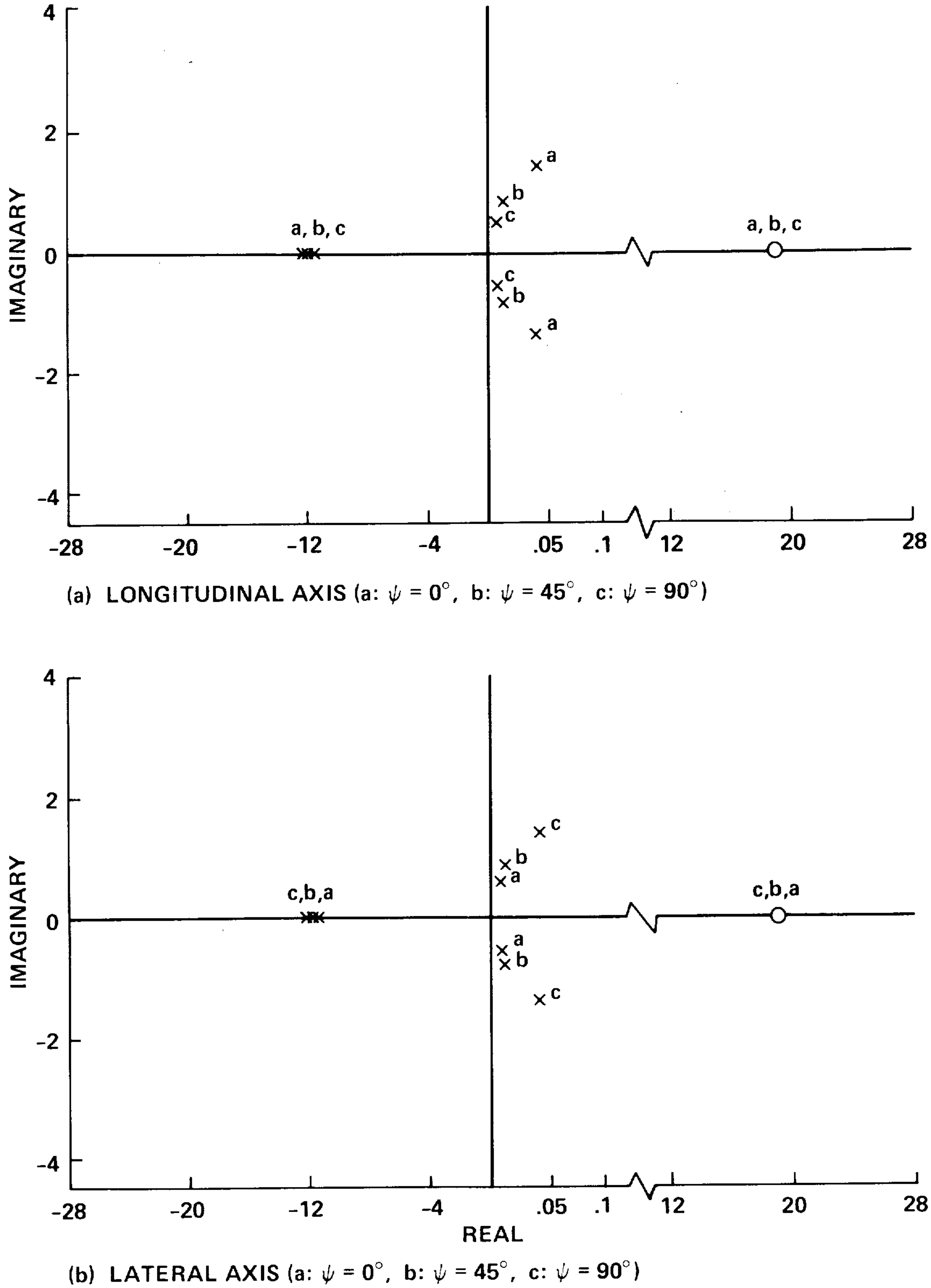

Figure 3.- Unaugmented stability analysis results. a. Longitudinal axis (a: $\psi = 0°$, b: $\psi = 45°$, c: $\psi = 90°$). b. Lateral axis (a: $\psi = 0°$, b: $\psi = 45°$, c: $\psi = 90°$).

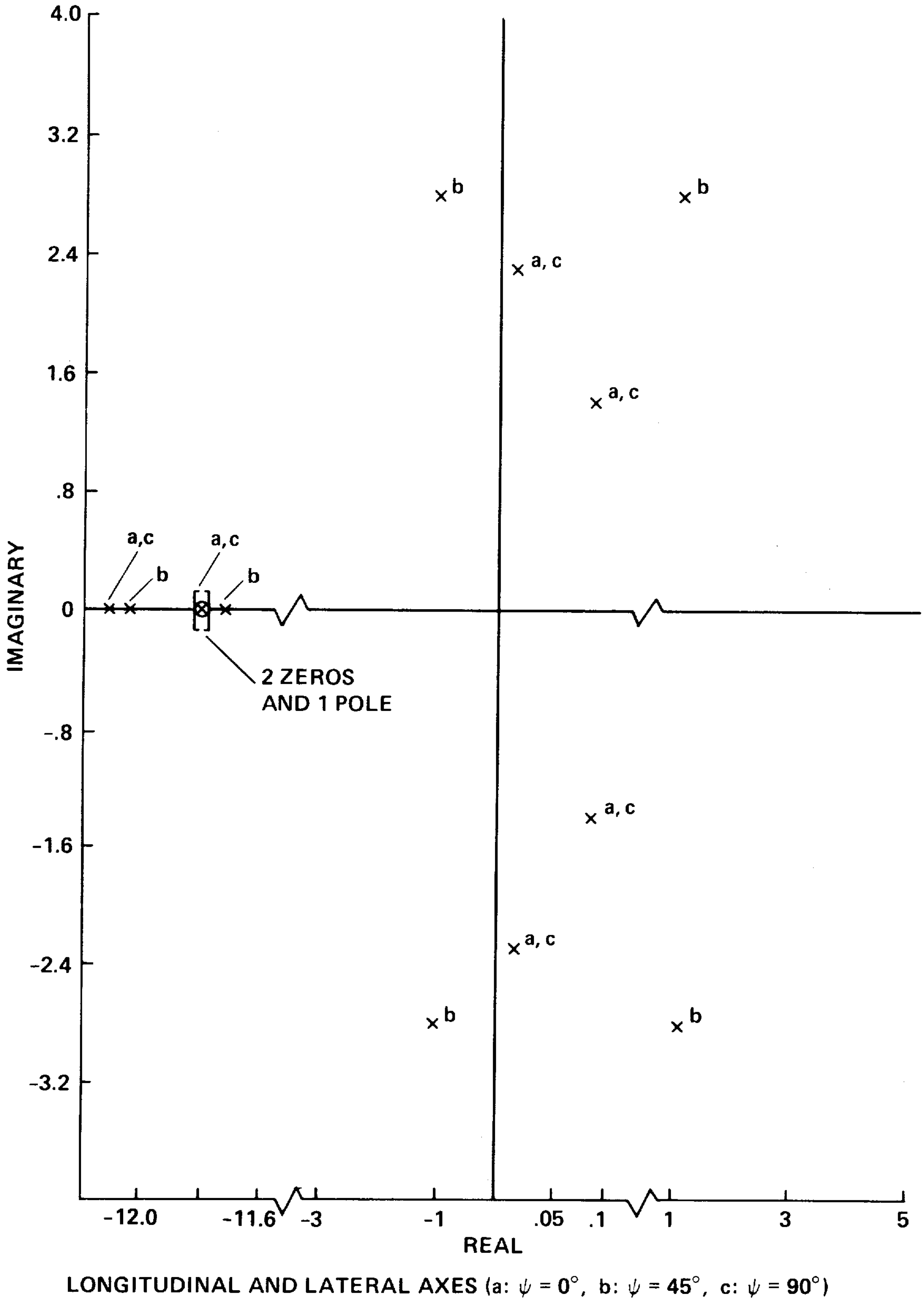

Figure 4.- Augmented stability analysis results.

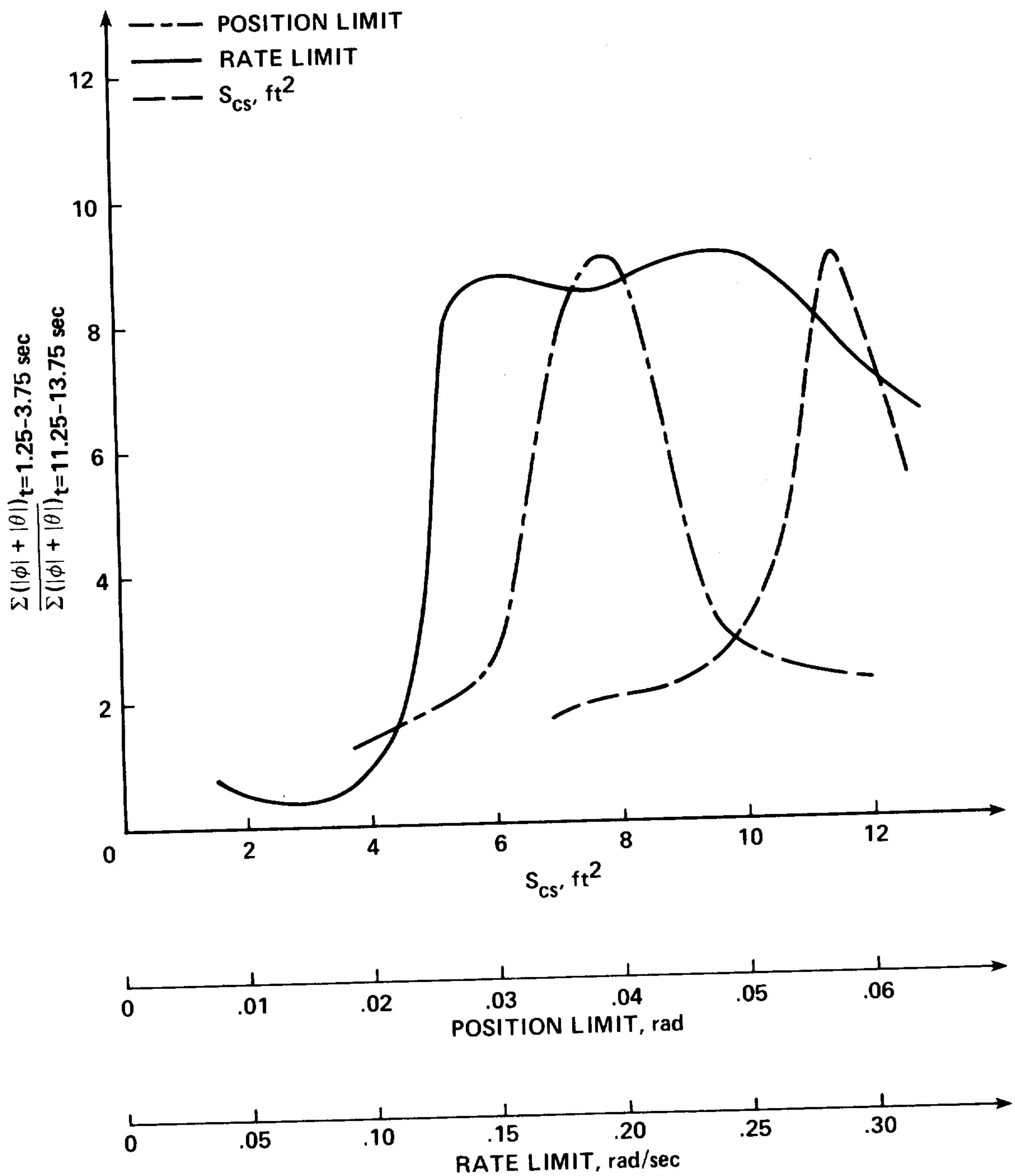

Figure 5.- Parameter variation results.

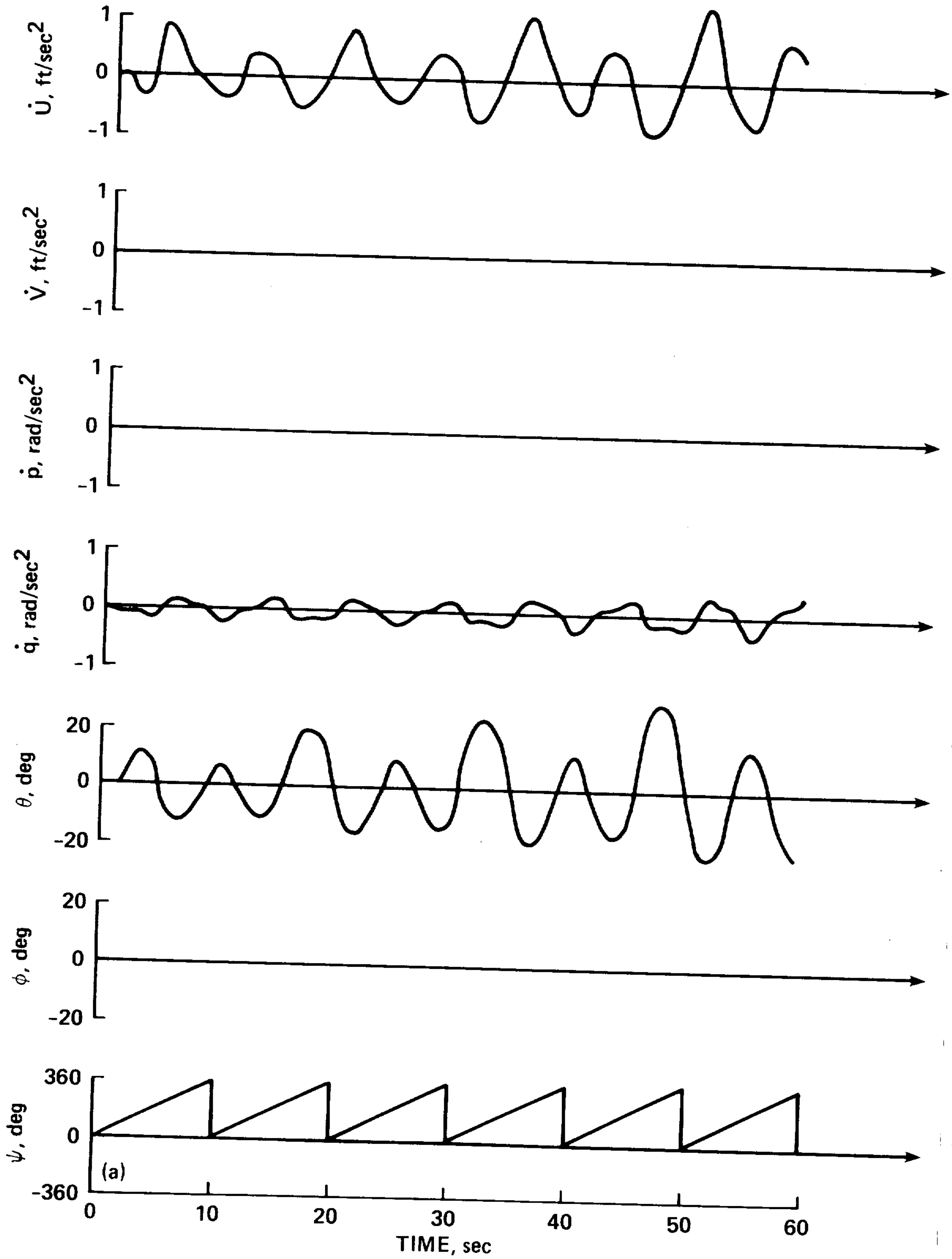

Figure 6.- Unaugmented numerical results.

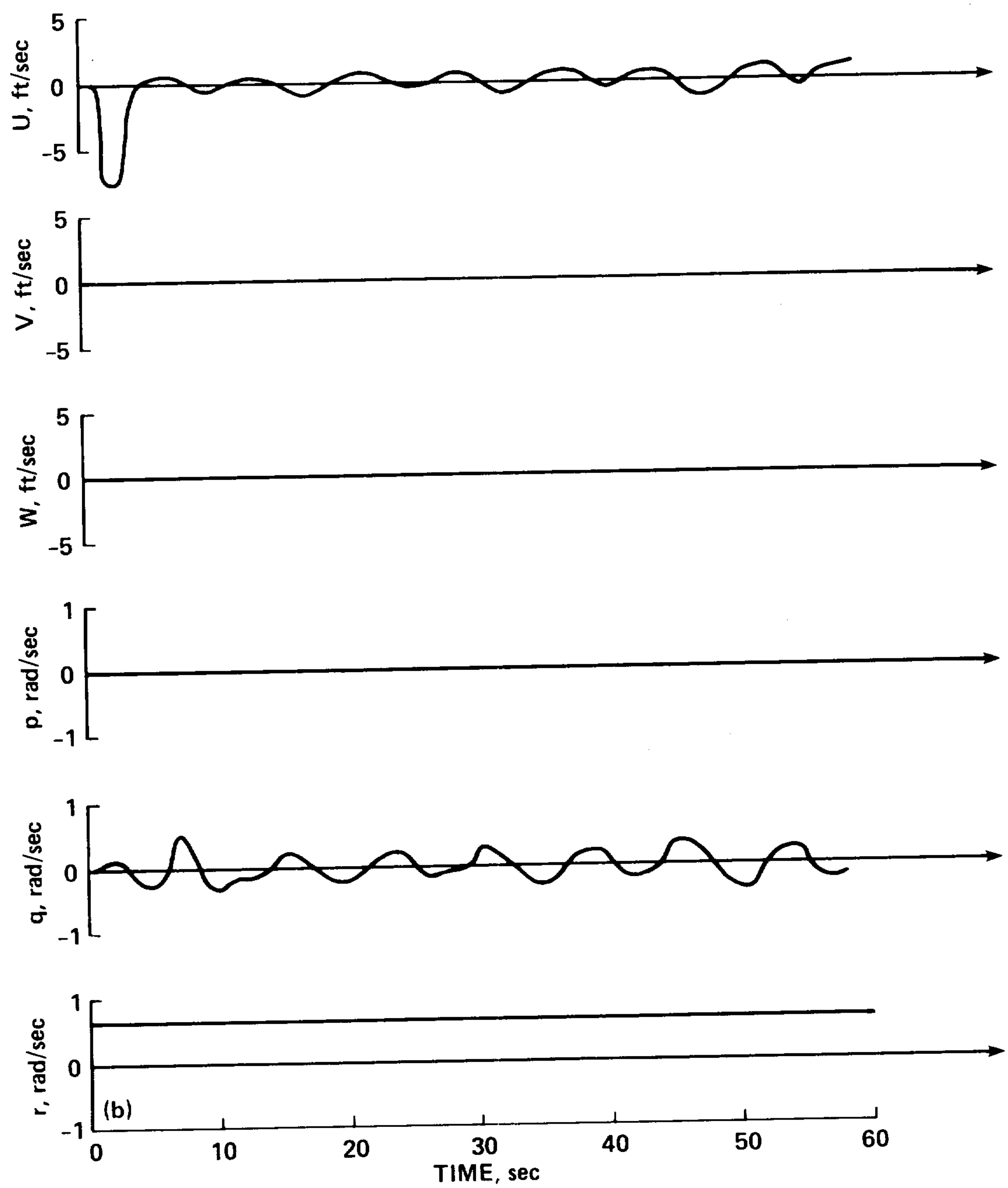

Figure 6.- Continued.

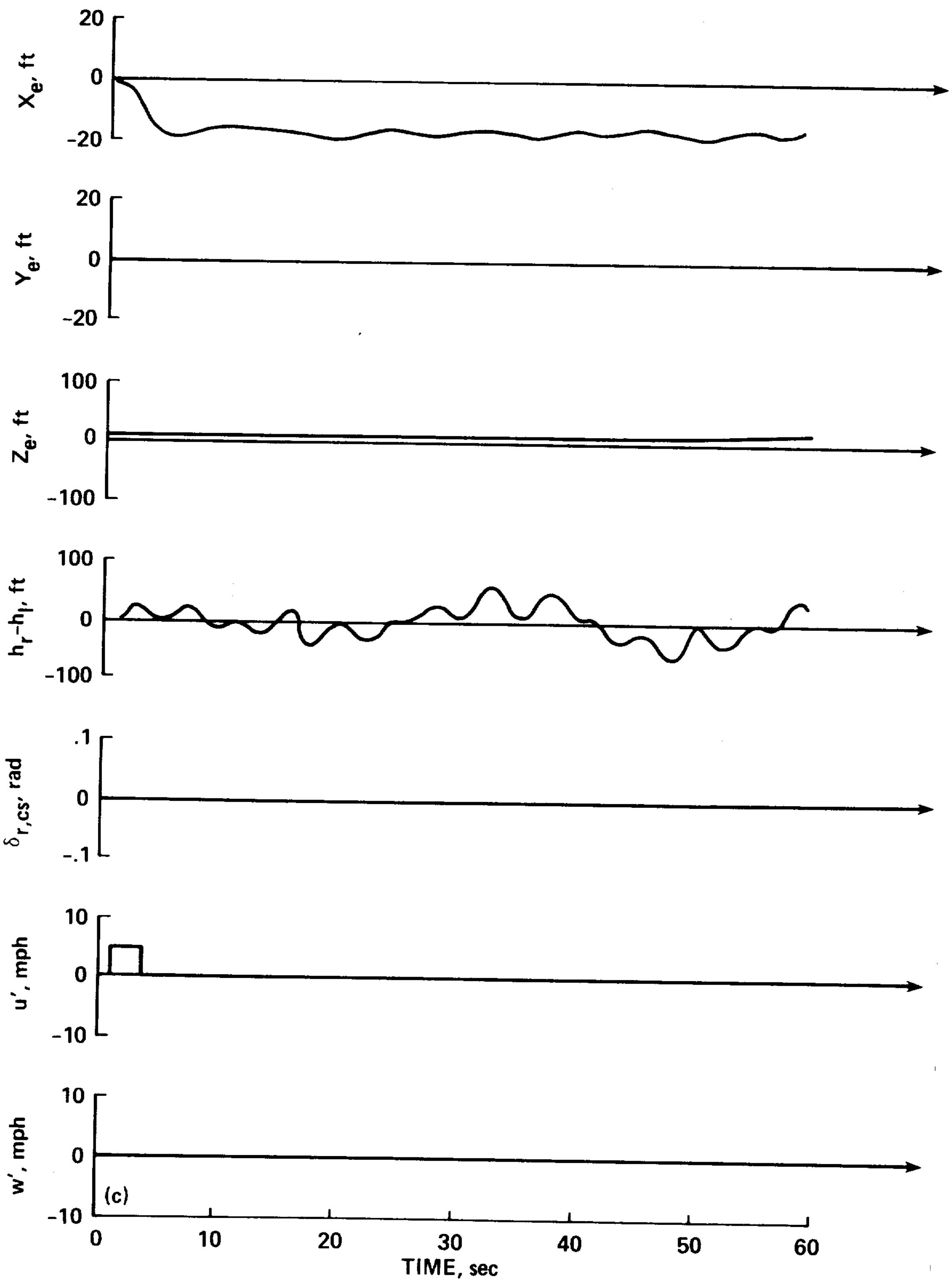

Figure 6.- Concluded.

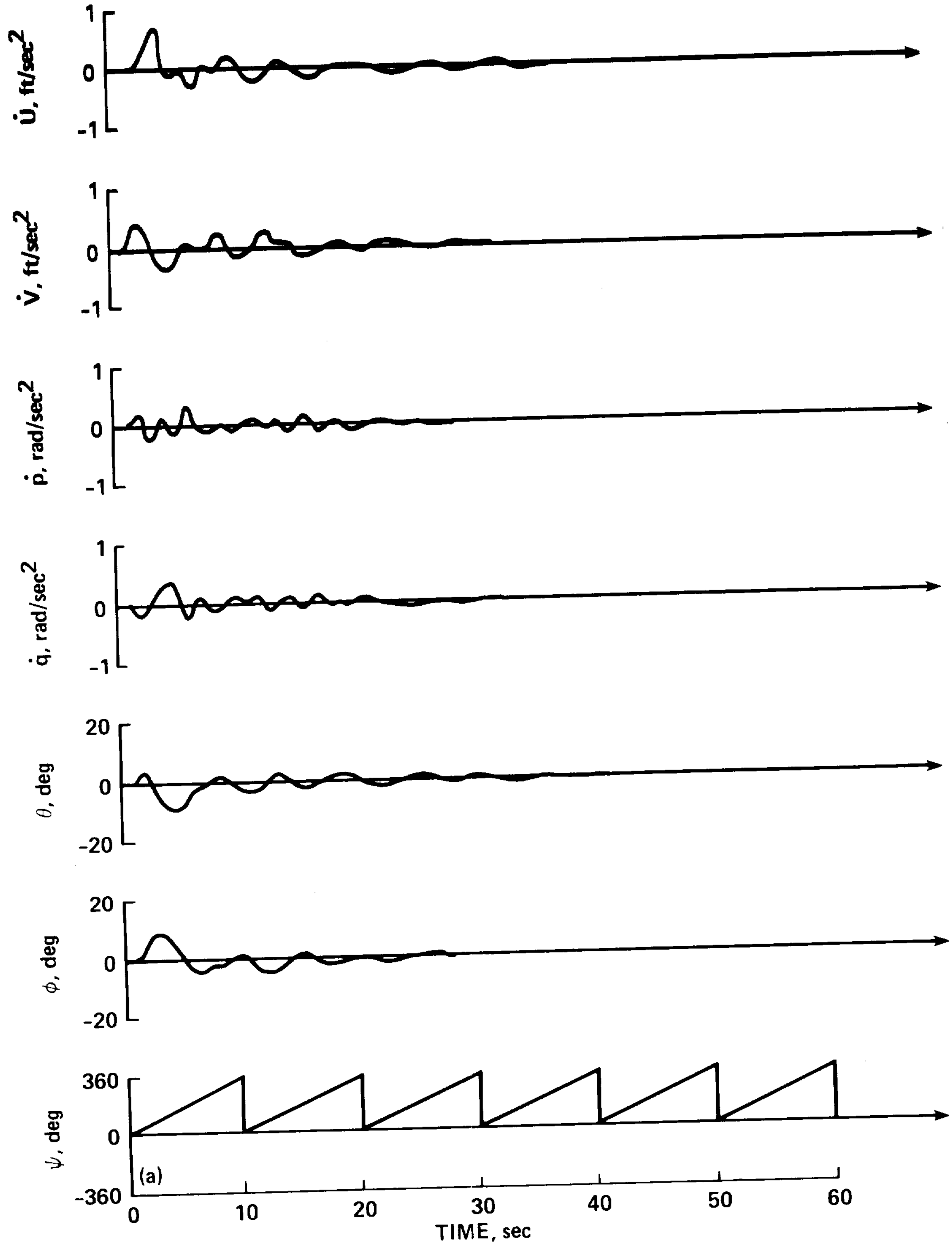

Figure 7.- Augmented numerical results without rate and position limiting.

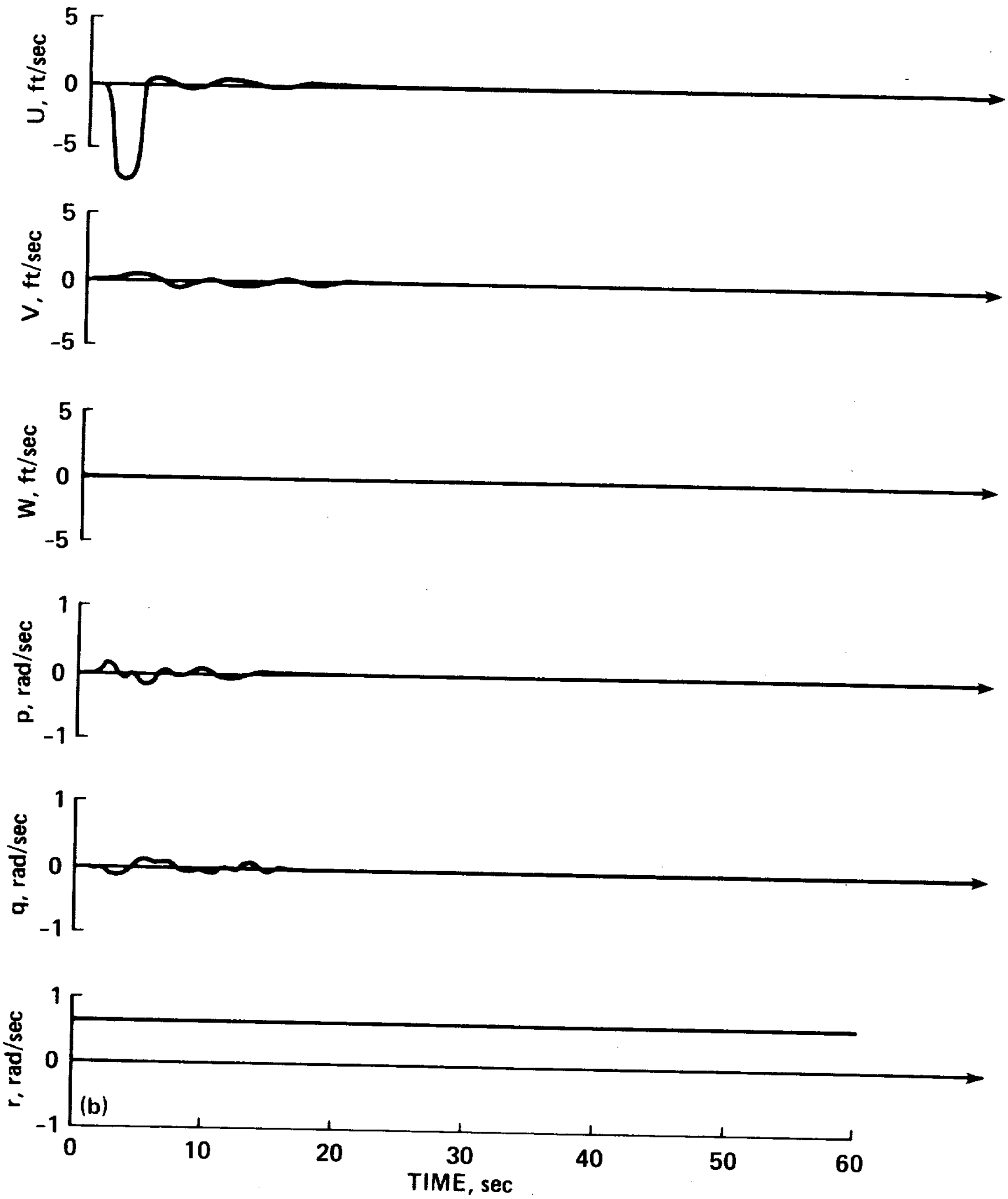

Figure 7.- Continued.

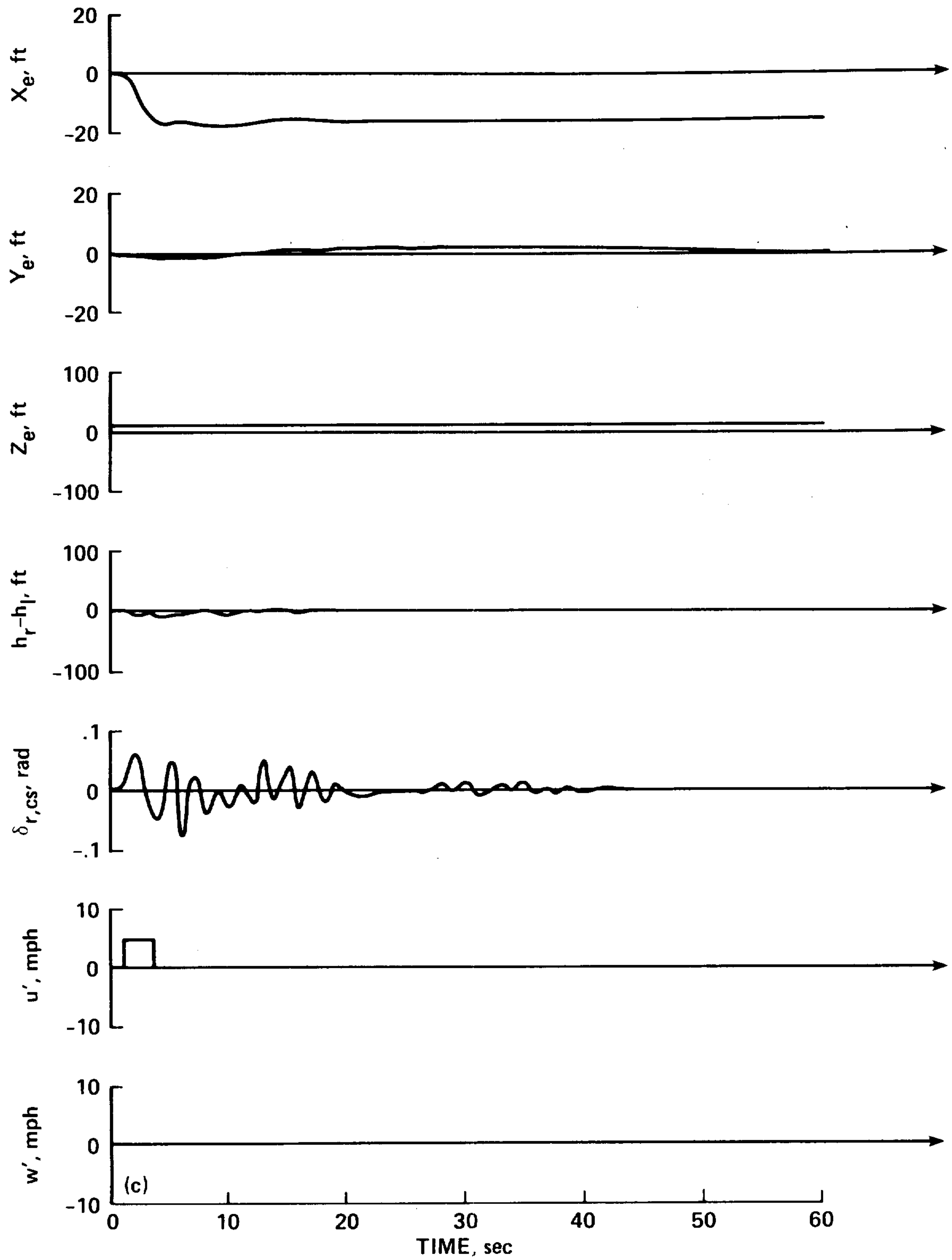

Figure 7.- Concluded.

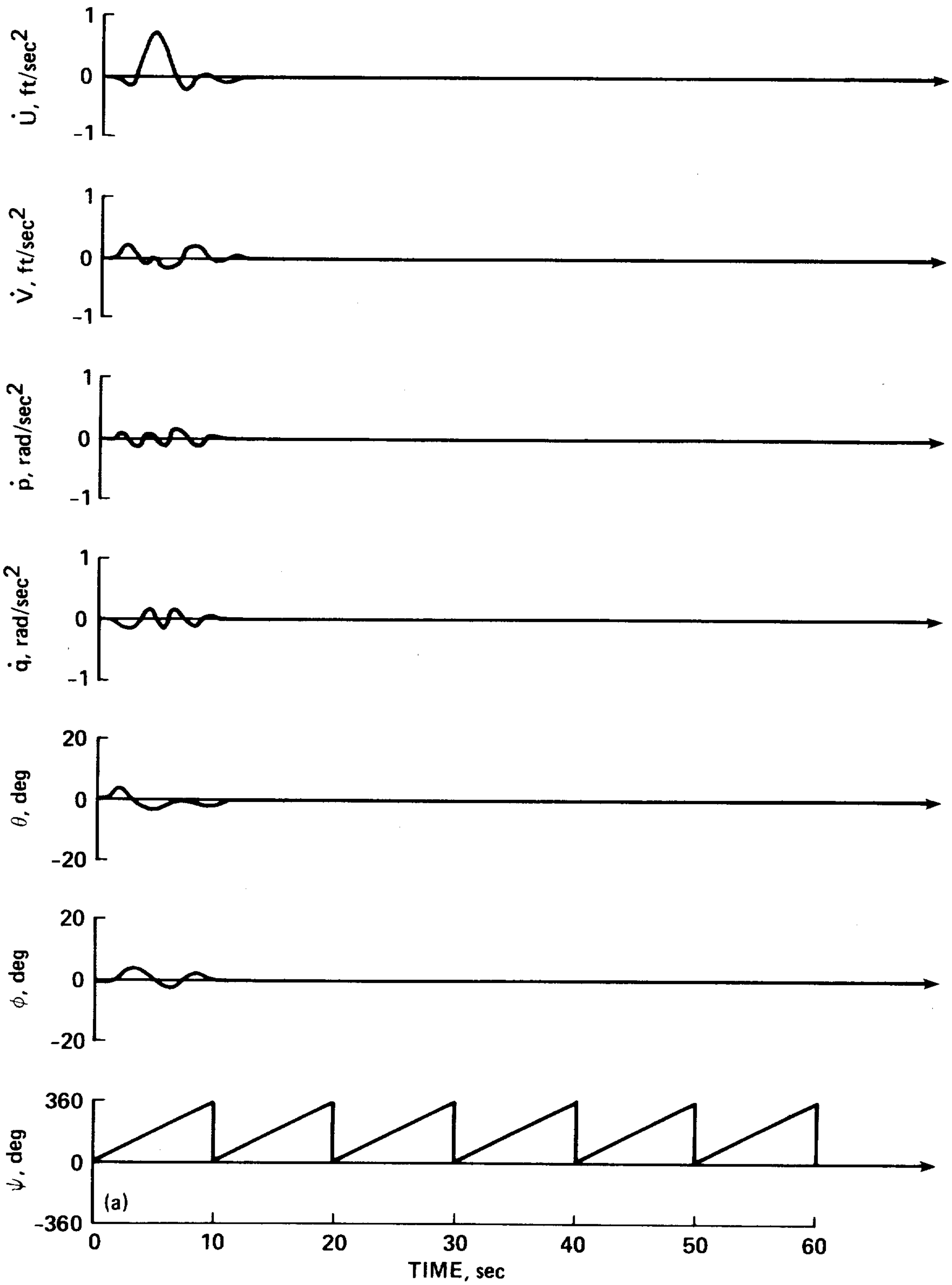

Figure 8.- Augmented numerical results.

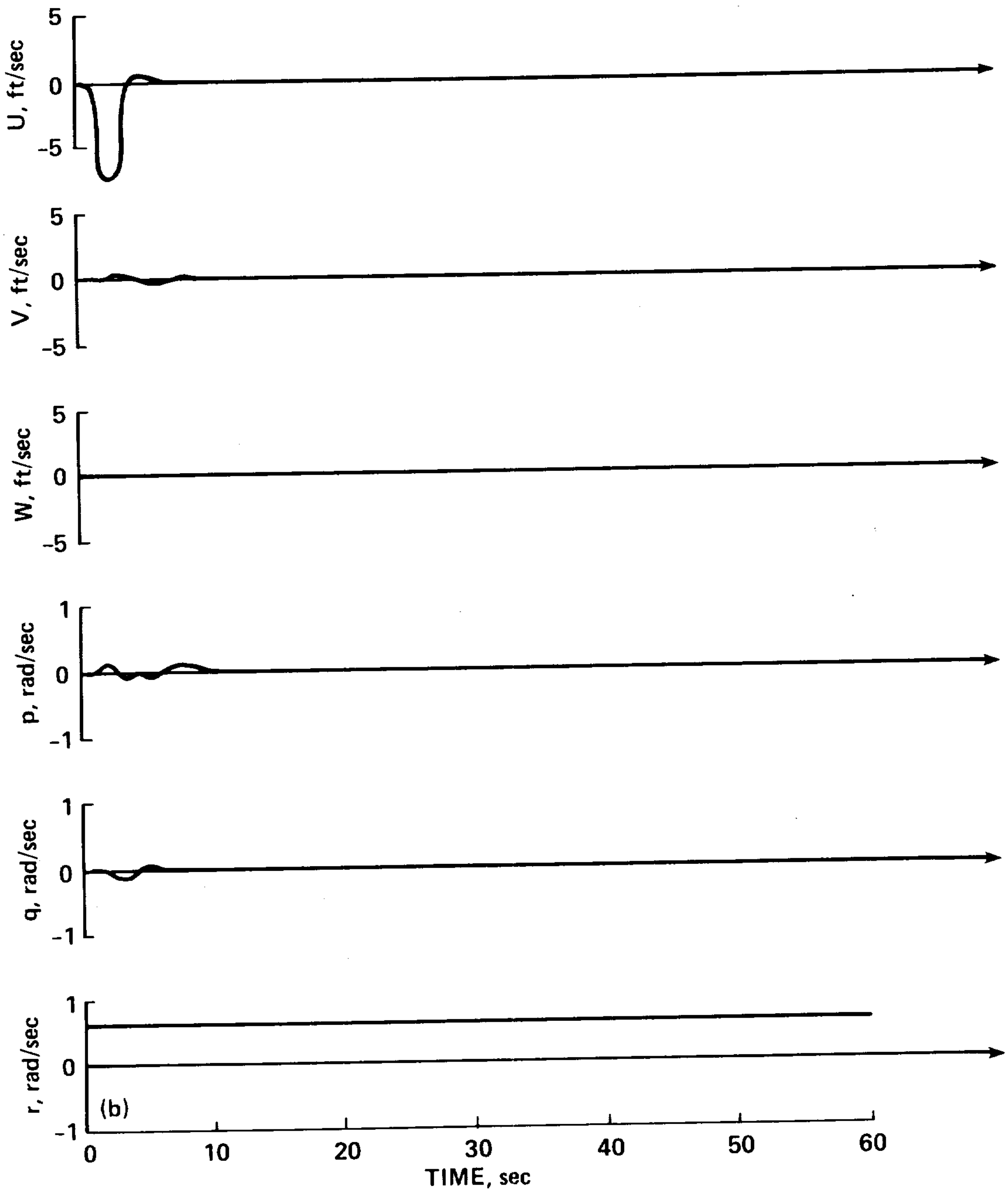

Figure 8.- Continued.

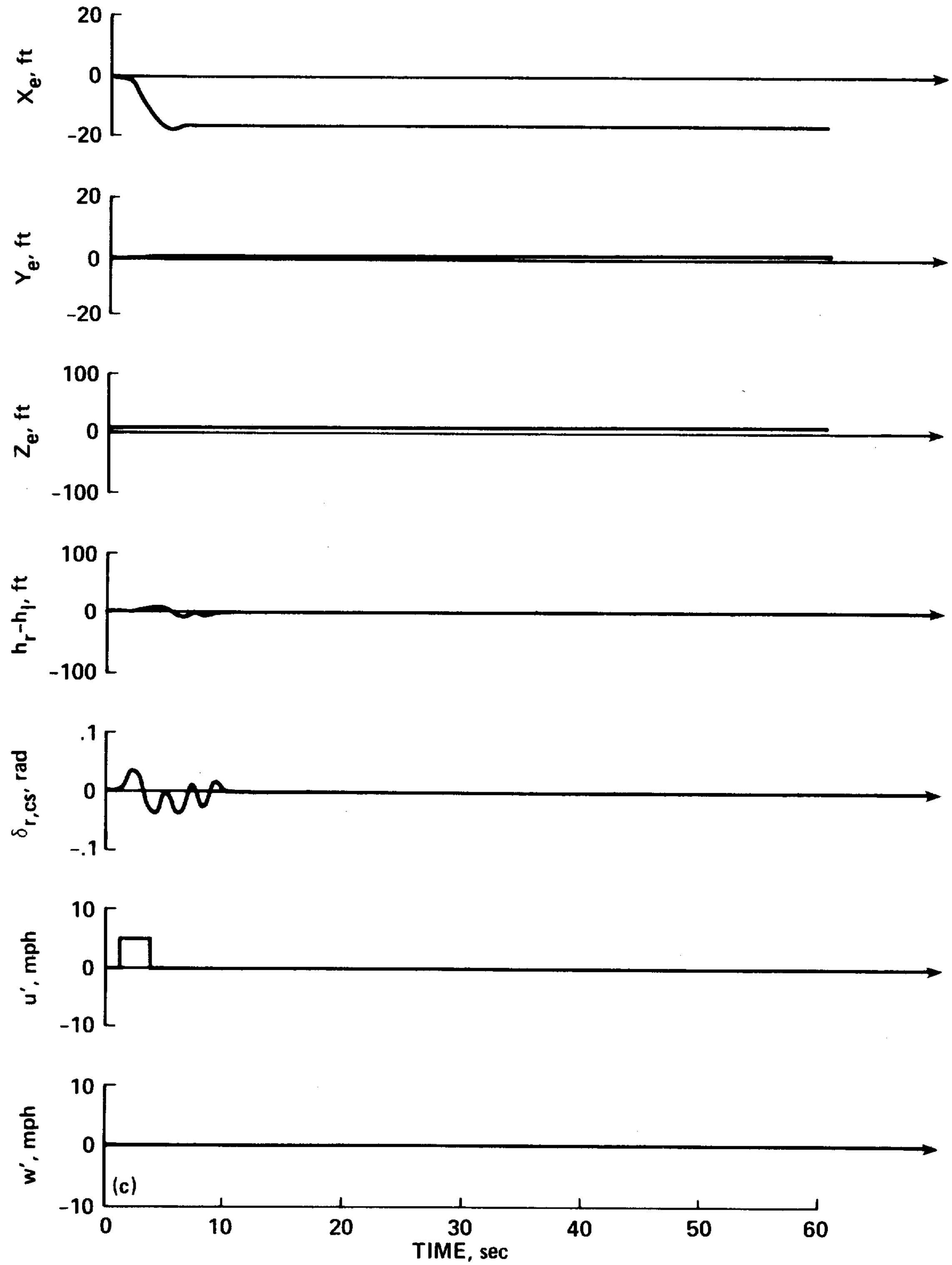

Figure 8.- Concluded.

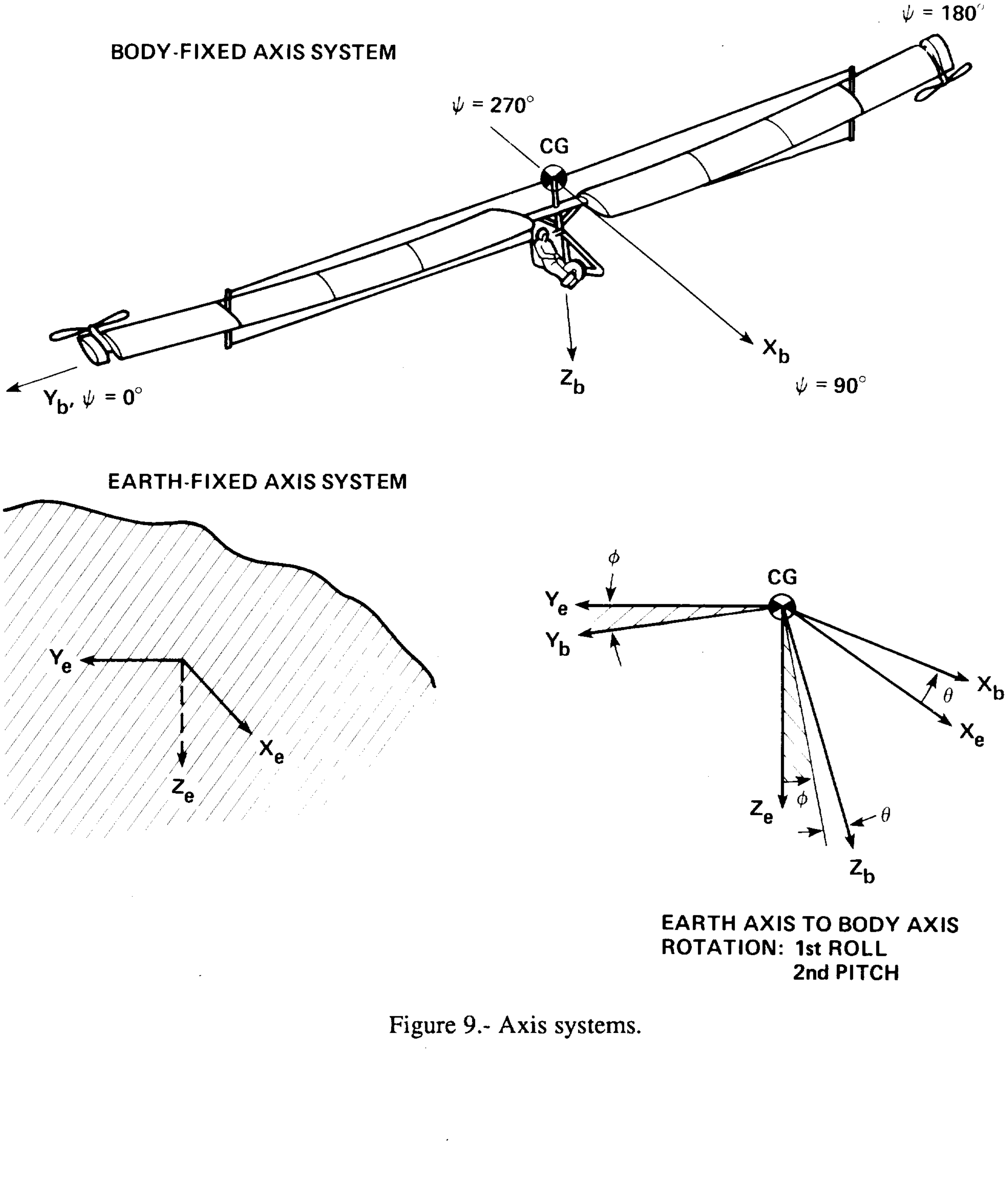

Figure 9.- Axis systems.

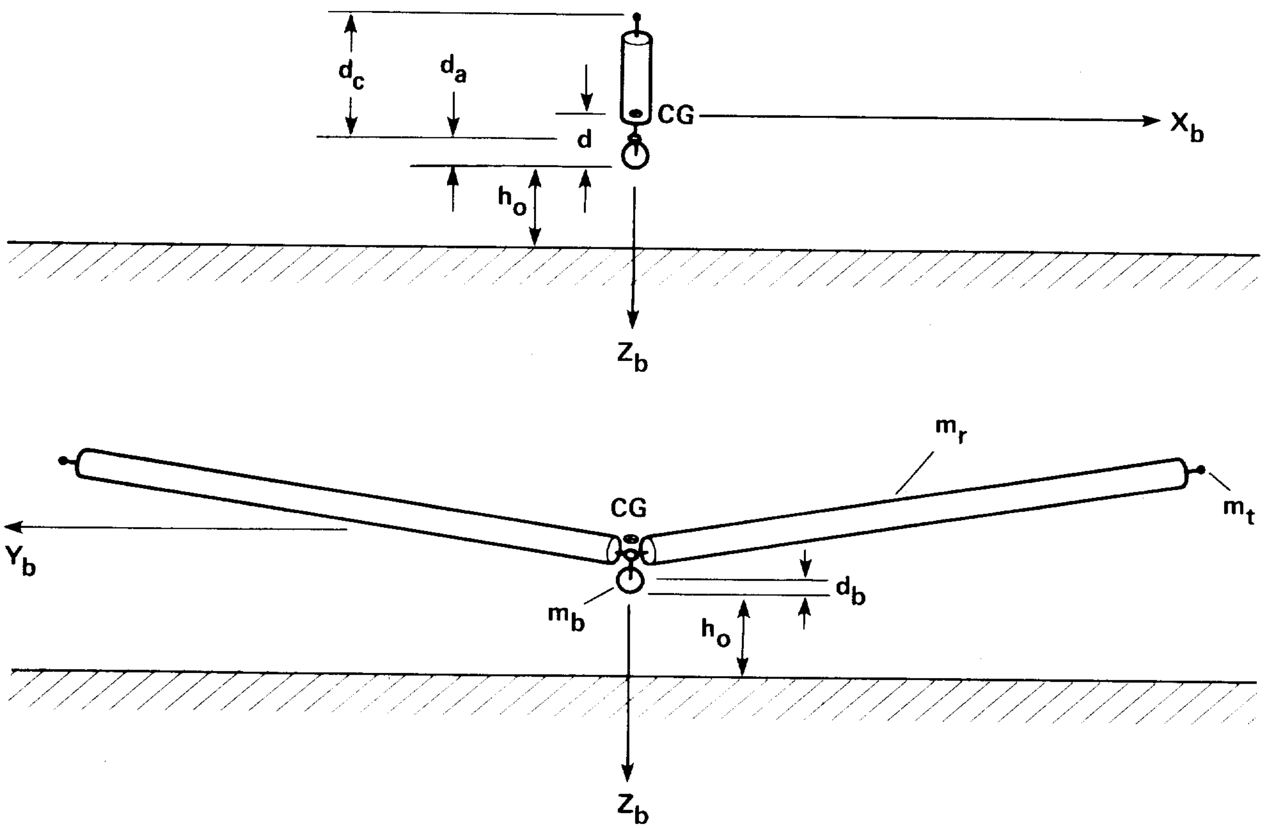

Figure 10.- Inertial representation.

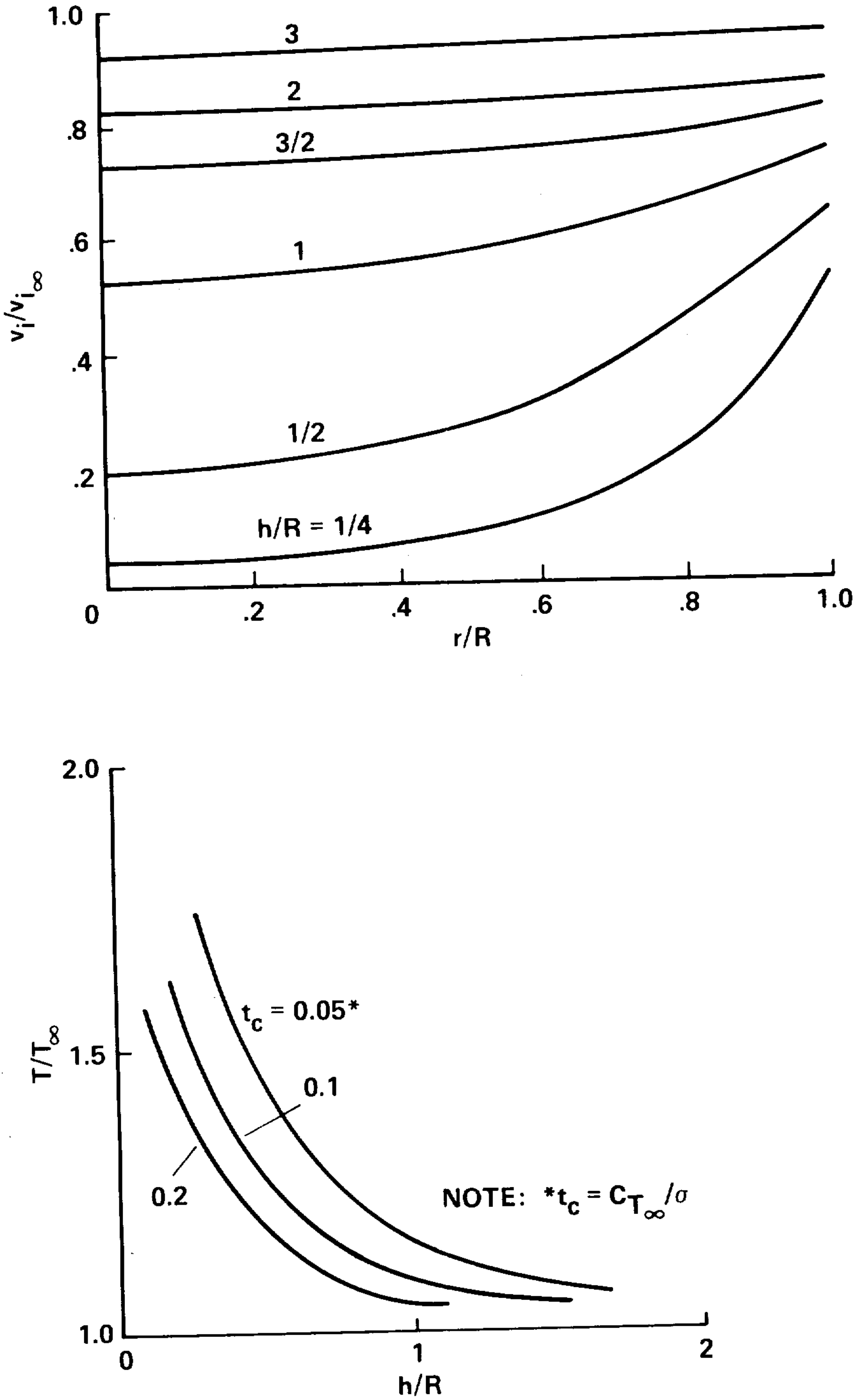

Figure 11.- Ground effect on thrust and induced velocity.

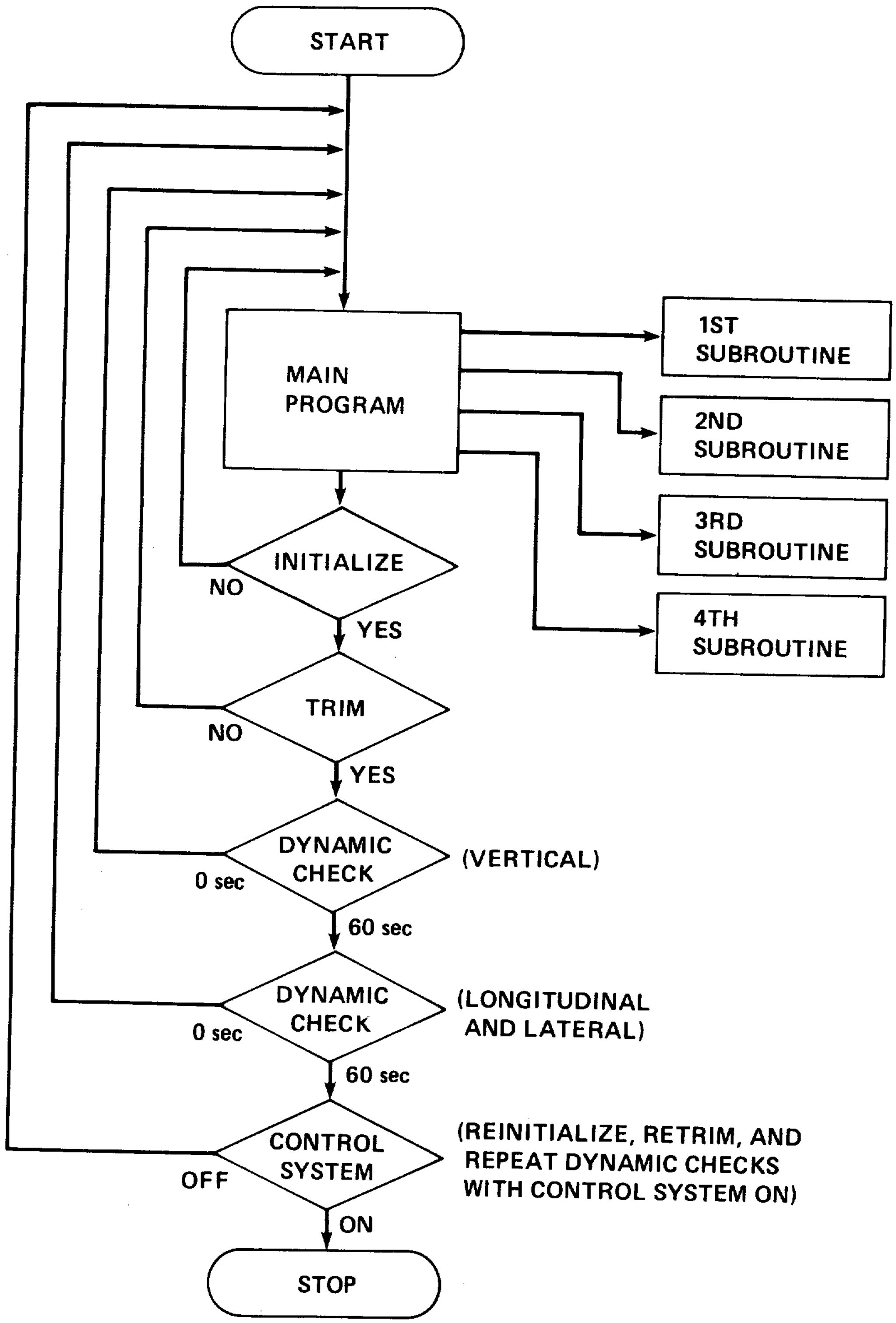

Figure 12.- Discrete simulation flow diagram.

NASA National Aeronautics and Space Administration

Report Documentation Page

1. Report No. NASA TM 101029	2. Government Accession No.	3. Recipient's Catalog No.
4. Title and Subtitle Control of a Human-Powered Helicopter in Hover		5. Report Date November 1988
		6. Performing Organization Code
7. Author(s) Joseph J. Totah and William Patterson (California Polytechnic State University, San Luis Obispo, CA)		8. Performing Organization Report No. A-88280
		10. Work Unit No. 505–67–29
9. Performing Organization Name and Address Ames Research Center Moffett Field, CA 94035		11. Contract or Grant No.
		13. Type of Report and Period Covered Technical Memorandum
12. Sponsoring Agency Name and Address National Aeronautics and Space Administration Washington, D.C. 20546-0001		14. Sponsoring Agency Code

15. Supplementary Notes

Point of Contact: Joseph J. Totah, Ames Research Center, MS-243-5, Moffett Field, CA 94035
(415) 694-6171 or FTS 464-6171

16. Abstract

This report documents the study of a control system for the Da Vinci II human-powered helicopter in hovering flight. This helicopter has two very large, slowly rotating rotor blades and is considered to be unstable in hover. The control system is designed to introduce stability in hover by maintaining level rotors through the use of rotor tip mounted control surfaces. A five degree of freedom kinematic model was developed to study this control system and is documented in this report. Results of this study show the unaugmented configuration to be unstable due to the large Lock Number, and the augmented configuration to be stable.

The role of the NASA in this study included the development and analysis of the kinematic model and control laws. Both analytical and numerical techniques were used.

17. Key Words (Suggested by Author(s)) Human-power, Helicopter, Hover, Control		18. Distribution Statement Unlimited – Unclassified. Subject Category: 08	
19. Security Classif. (of this report) Unclassified	20. Security Classif. (of this page) Unclassified	21. No. of pages 60	22. Price A02

NASA FORM 1626 OCT 86

For sale by the National Technical Information Service, Springfield, Virginia 22161